Water usage of old growth oak at elevated CO_2 in the FACE of climate change.

Susan E. Quick[1 2], Giulio Curioni[1 2], Nicholas J. Harper[2], Stefan Krause[1 2 3 4], A. Robert MacKenzie [1 2]

[1]School of Geography, Earth and Environmental Sciences, University of Birmingham, Birmingham, B15 2TT, UK
[2]Birmingham Institute of Forest Research, University of Birmingham, Birmingham, B15 2TT, UK
[3]Laboratoire d'ecologie des hydrosystemes naturels et anthropises, University Claude Bernard, Lyon1, Lyon, France (LEHNA)
[4]Institute for Global Innovation, University of Birmingham, Birmingham, B15 2TT, UK

Correspondence to: (Susan E. Quick (SEQ616@student.bham.ac.uk) - proofs etc. only), A. Robert MacKenzie (A.R.Mackenzie@bham.ac.uk) official correspondence author

Abstract.

Predicting how increased atmospheric CO_2 levels will affect water usage by whole mature trees remains a challenge. The present study investigates diurnal (i.e. daylight) water usage of old growth oaks within an experimental treatment season April–October inclusive. Over five years, 2017–2022, we collected individual tree data from eighteen oaks (*Quercus robur L.*) within a large-scale manipulative experiment at the Birmingham Institute of Forest Research (BIFoR) Free-Air CO_2 Enrichment (FACE) temperate forest in central England, UK. Diurnal tree water usage per day (*TWU*, litres d^{-1}) across the leaf-on seasons was derived from these data. Six trees were monitored in each of three treatments: FACE infrastructure arrays of (+150 µmol mol^{-1}) elevated CO_2 (eCO_2); FACE infrastructure control ambient CO_2 (aCO_2) arrays; and control *Ghost* (no-treatment-no-infrastructure) arrays. For each tree, sap flux demonstrated a circumferential imbalance across two stem orientations. Median and peak (95%ile) diurnal sap flux and *TWU* increased in the spring from first leaf to a broad summer maximum (July−September) and declining more slowly towards full leaf senescence (October−November). Water usage varied between individual oaks by size. *TWU* was linearly proportional to tree bark radius, R_b (ca. 3.1 litres d^{-1} mm^{-1}, 274 mm ≤ R_b ≤ 465 mm). R_b was also a very good proxy for projected canopy area, A_c (m^2), which was linearly proportional to R_b (ca. 617 m^2 m^{-1}). ~~This~~Applying the stem-to-canopy relation implied a mean July water usage of ca. 5 litres d^{-1} m^{-2} of oak canopy in the BIFoR FACE forest. We normalised *TWU* by individual tree R_b, which we call TWU_n (litres d^{-1} mm^{-1}). We report whole-season treatment effects, differing year on year, alongside July-only results. In 2019 and 2021 seasons, there was a ~~13.9~~14–19%, reduction in eCO_2 TWU_n compared with aCO_2 TWU_n, with a marginal 3% reduction in 2020. In July 2019 there was a 26% reduction in TWU_n under eCO_2 treatment, but no significant differences in other July data. Control trees exhibited 20–37% increase in aCO_2 TWU_n compared with *Ghost* TWU_n consistently in whole-seasons and July-only comparisons (~~9.9~~10–48% increase) during 2019−2021. Several factors may contribute: the installation or operation of FACE infrastructure; array-specific differences in soil moisture, slope, soil respiration; or the mix of sub-dominant tree species present. Our results of normalised per-tree water savings under eCO_2 align with sap flow results for other FACE experiments and greatly extend the duration of observations for oak, elucidating seasonal patterns and interannual differences. Our tree-centred viewpoint complements leaf-level and ground-based measurements to extend our understanding of plant-water usage in old growth oak forest.

1 Introduction

Long-term manipulation experiments enable prediction of how, under climate change, increased atmospheric carbon dioxide levels and climate extremes might affect plants and ecosystems. Plant hydraulics are adapted to expected ranges of environmental parameters, with larger plants exhibiting greater resilience to wider parameter variation due to their ability to maintain water and food reserves. Large trees can maintain their transpiration rates even during water stress but remain vulnerable (Süßel and Brüggemann, 2021). To maintain transpiration demands, trees accommodate to: diel variation in solar radiation; respiration fluctuation; high temperatures; and seasonal soil water deficits. Short-term mechanisms include stomatal regulation, stem diameter variations (Sánchez-Costa et al., 2015), use of stored plant water, and use of available water at variable soil depth (David et al., 2013; Flo et al., 20211; Gao and Tian, 2019; Nehemy et al., 2021). Longer term strategies include development of resilient root structures (David et al., 2013; Flo et al., 2021) and minimisation of embolism mitigated by different xylem structures (Gao and Tian, 2019). The ability of mature trees to withstand climate extremes may rely in part on using these buffering traits which act to prevent permanent damage and maintain viability (Iqbal et al., 2021; Moene, 2014). This prompts the further question of how increasing atmospheric carbon dioxide levels will affect the hydraulic resilience of trees. (section 1.1, below).

The response of woody plants to drought varies considerably by species (Leuzinger et al., 2005; Vitasse et al., 2019), location (e.g. north versus south in Europe (Stagge et al., 2017)), soil characteristics such as soil texture (Lavergne et al., 2020) and combinations thereof (Fan et al., 2017; Salomón et al., 2022; Sulman et al., 2016; Venturas et al., 2017). Trees require water/ water vapour at all stages of life experiencingand experience insufficient water at times (e.g. under elevated temperatures and drought)), so tree species have evolved different root traits (Montagnoli, 2022) and hydraulic characteristics (Sperry, 2003) to maintain their fitness to their environment. Volkmann et al., (2016) used rainwater isotopes to track soil water sources for sessile oak (*Quercus petrea*) and beech (*Fagus sylvatica*). Sánchez-Pérez et al., (2008) studied oak (*Quercus robur*), ash (*Fraxinus excelsior)* and poplar (*Populus alba*). Both studies found that use of soil water at different depths varied between species and seasonal variation of climatic conditions. Trees therefore exhibit variable resilience to water shortage/ excess and other environmental stressors (Brodribb et al., 2016; Choat et al., 2018; Grossiord et al., 2020; Landsberg et al., 2017; Martínez-Sancho et al., 2022; Niinemets and Valladares, 2006; Schäfer, 2011; Süßel and Brüggemann, 2021) with a broad spectrum of sometimes species-specific strategies and coping mechanisms (Schreel et al., 2019).

1.1 Future-forest atmospheric carbon dioxide and water usage

Primary producers may respond to elevated CO_2 (eCO_2) levels by assimilating and storing more carbon, which for plants containing chlorophyl happens during photosynthesis. Global carbon and water cycle models (Guerrieri et al., 2016; De Kauwe et al., 2013; Medlyn et al., 2015; Norby et al., 2016) predict that, at least until the middle of the 21st century, trees and plants could potentially -photosynthesise more efficiently, which may induce increased carbon storage. This could be beneficial for individual tree productivity. Stomatal regulation determines the trade-offs between carbon assimilation and water loss and, for a given leaf area and stomatal density, determines the rate and quantity of water usage seen in the stems of woody plants. Water usage at tree level is, therefore, a strongly integrative measure of the whole plant response to environmental drivers (such as temperature and precipitation) and experimental treatments (such as eCO_2).

Untangling the canopy water exchange and soil moisture hydraulic recharge dynamics within forest Free-Air CO_2 Enrichment (FACE) experiments can be complex, but responses to eCO_2 manipulations (including stepwise

increases (Drake et al., 2016)) inform our understanding of plant responses to climate change scenarios. Specific studies concerning transpiration and water savings of eCO_2 responses (Ellsworth, 1999; Li et al., 2003) have already improved the model predictions (De Kauwe et al., 2013; Donohue et al., 2017; Warren et al., 2011a) and here we seek improvements to mechanistic process understanding that will enable further advances to predictive model capacity.

Experimental research into ecohydrological responses of old growth deciduous forest to changing atmospheric CO_2 levels has been limited. The Web-FACE study (Leuzinger and Körner, 2007) reported on temperate old growth species and found that eCO_2 reduced water usage in *Fagus sylvatica* L. (dominant) and *Carpinus Betula* L. (subdominant) by about 14% but had no significant effect on the water usage of *Quercus petraea* (Matt.) Liebl., the other dominant species present. There were a small number of trees (six) of a Quercus species included in Leuzinger and Körner's (2007) study, with water savings monitored by accumulated sap flux (normalised against peak values in each tree) over two 21-day periods. Changes in water usage by old growth oak trees at eCO_2 when measuring for longer periods (greater than a month) across the leaf-on season have not previously been reported. The paucity of studies of the water usage of mature temperate trees under eCO_2 significantly weakens model-data comparisons at FACE sites (De Kauwe et al., 2013). Warren et al., (2011a) reviewed the forest FACE experiments which, apart from Web-FACE, all constituted younger deciduous and mixed plantations less than thirty years old (Schäfer et al., 2002; Tricker et al., 2009; Uddling et al., 2008; Wullschleger & Norby, 2001; Wullschleger et al., 2002). Some of these studies are long-term (> ten years) but all are limited in their period of monitoring sap flow, maximum continuous data periods being covered by Schäfer et al., (2002) at Duke forest USA (1997-2000) and lesser periods by Oak Ridge National Environmental Research Park (ORNL) USA and POP/ EuroFACE (Wullschleger & Norby, 2001; Tricker et al., 2009). Larger numbers of young trees (252 aspen–birch) were monitored for sap flux by Uddling et al., (2008), whereas most recent sap flow studies of oak have either been single trees of different species (e.g. Steppe et al., 2016) or short-term proof-of-concept studies using experimental instrumentation (Asgharinia et al., 2022).

There are further (2010 onwards) sap studies of deciduous oak which do not manipulate CO_2 but which offer helpful data for comparison, for example within Europe (Aszalós et al., 2017; Čermak et al., 1991; Hassler et al., 2018; Perkins et al., 2018; Schoppach et al., 2021; Süßel and Brüggemann, 2021; Wiedemann et al., 2016) and North America (Fontes and Cavender-Bares, 2019). Robert et al. (2017) have reviewed the characteristics of these old growth species from multiple studies which help us to place our results in context. Within the UK maritime temperate climate, only a few ecohydrological studies (e.g. Herbst et al., 2007; Renner et al., 2016) have previously considered the sap flow responses to water availability and drought for old growth Quercus species.

The FACE method was developed to eliminate chamber/infrastructure influences (Pinter et al., 2000; Miglietta et al., 2001), and provides good control over CO_2 elevation levels (e.g. Hart et al., 2020). Nevertheless, few studies have explored the effects of the experimental infrastructure on the resulting microclimate (LeCain et al., 2015). Disturbance of the vegetation was kept to a minimum while constructing BIFoR FACE (Hart et al., 2020) but some clearing of ground flora and removal of coppice stems did occur plausibly reducing competition and making more soil water available to the oaks. Other possible effects of infrastructure on water availability are discussed in section 3.5.2.

1.2 Improving global vegetation models and questions of scale.

Global vegetation models have been developed based on leaf-level plant knowledge alongside that of soil-tree-atmosphere exchange (e.g. Medlyn et al., 2015). These models have predicted reduced canopy conductance, G_s

and increased run-off in future climate scenarios, but an important gap has been identified between estimated and observed water fluxes (De Kauwe et al., 2013).

Canopy/ leaf transpiration estimates from stem xylem sap flux (Granier et al., 2000; Wullschleger and Norby, 2001; Wullschleger et al., 2002), use the parameter canopy conductance (*Gs*) to reflect how the whole canopy transpires rather than concentrating on individual leaf stomatal conductance to water. Measurements of *Gs* and transpiration and partitioning of evapotranspiration in deciduous forests (Tor-ngern et al., 2015; Wehr et al., 2017) have now clarified relationships between canopy parameters and environmental variables PAR, VPD and precipitation. Long-term carbon and water flux data from flux towers in forest ecosystems (e.g. Ameriflux (Baldocchi et al., 2001), Euroflux (Valentini, 2003), FluxNet (Baldocchi et al., 2005)) and satellite datasets such as EOS/Modis worldwide (Huete et al., 1994), have provided canopy level and landscape wide data. ~~Plant focused~~Field based environmental manipulation studies, such as FACE, can provide data on individual parameters and processes to inform and challenge the models.

At the forest scale, studies of the effects of ~~the~~ European drought (2018-2019) on forested landscapes have shown that recovery time for surviving trees may be several years, affecting both plant growth, stem shrinkage (Dietrich et al., 2018) and branch mortality during that time, especially for ~~old growth~~ deciduous species in mature or old-growth forests (Salomón et al., 2022). At this forest scale (Keenan et al., 2013; Renner et al., 2016), there is also a more complex impact on ecosystem and atmospheric demands as planetary-scale CO_2 levels increase, affecting boundary layer feedbacks.

In contrast to forest- and leaf-scale studies, the present study is tree-focused and bridges the data gaps identified previously (De Kauwe et al., 2013; Medlyn et al., 2015) in respect of model-data scale mismatch. Tree-scale studies have provided essential data for calibration and validation of tree-water models (De Kauwe et al., 2013; Wang et al., 2016;), identified key parameters driving responses to expected water shortages (Aranda et al., 2012) and compared species differences in mature tree responses to ambient (Catovsky et al., 2002) or eCO_2 (Catoni et al., 2015; Tor-ngern et al., 2015). Xu and Trugman, (2021) have updated the previous empirical parameter approach to global vegetation modelling, reinforcing the need to use measured tree parameters (such as sapwood area) to improve model predictions of climate change response.

Here we focus on whole ~~-~~tree ~~species traits~~species' characteristics and link these parameters to diurnal (i.e. daylight) tree water usage per day (*TWU*, litres d^{-1}) from stem xylem sap measurements, affirming the ~~-~~influence of leaf-on season precipitation and solar radiation/ air temperature. Measurements of xylem sap flux are marginally intrusive, providing highly time-resolved data of plant water usage for several years with minimal maintenance. Heat-based measurement techniques (Forster, 2017; Granier et al., 1996; Green & Clothier, 1988) have been used over the past 40 years for measurements of plant xylem hydraulic function (Landsberg et al., 2017; Steppe and Lemeur, 2007), with automated data capture enabling increasingly realistic models of whole tree xylem function.

1.3 Objectives, research questions and hypotheses

This study provides new ~~gap filling~~ data to characterise seasonal and inter-year patterns of daily water usage by old growth oak trees ~~using monthly distributions.~~under elevated CO2 and taking into account the effect of FACE infrastructure. We test for significant differences between treatments within these water usage distributions and patterns. The paper examines the limitations of water usage measurement by compensation heat pulse (HPC) sap transducers. It also relates diurnal tree water usage per day (*TWU*, litres d^{-1}) to measurable tree traits (bark radius, R_b (mm) and canopy area, A_c (m^2)) and examines variation of *TWU* with environmental drivers and soil moisture. The following specific research questions and associated hypotheses are considered:

1. Is there a measurable difference in *TWU* distribution under eCO_2 compared to (infrastructure-containing) ambient CO_2 control (aCO_2) across the seasonal cycle?

Hypothesis 1: A detectable eCO_2 treatment effect on *TWU* is present.

2. Does the presence of FACE infrastructure measurably affect *TWU*?

Hypothesis 2: *TWU* is greater in the presence of FACE infrastructure.

2 Materials and Methods

2.1 BIFoR FACE

At the Birmingham Institute of Forest Research (BIFoR) FACE experiment in central England, UK, (Hart et al., 2020), we investigate soil-plant-atmosphere flows and fluxes of energy and water (Philip, 1966). We monitor soil-xylem-stomatal responses to aCO_2 and eCO_2 levels in a mixed deciduous temperate forest of approximately 180-year-old trees. The eCO_2 treatment represents conditions expected by the middle of the 21st century (see shared socioeconomic pathways (SSPs) in IPCC, 2021). This long-term experiment presents a rare opportunity to gain new insight into the complexity of water usage of old growth trees in a changed atmospheric composition. BIFoR FACE is unique amongst free-air experiments in its ability to study the ecohydrology of old growth pedunculate oaks (*Quercus robur L.*, subsequently abbreviated to oak) under eCO_2.

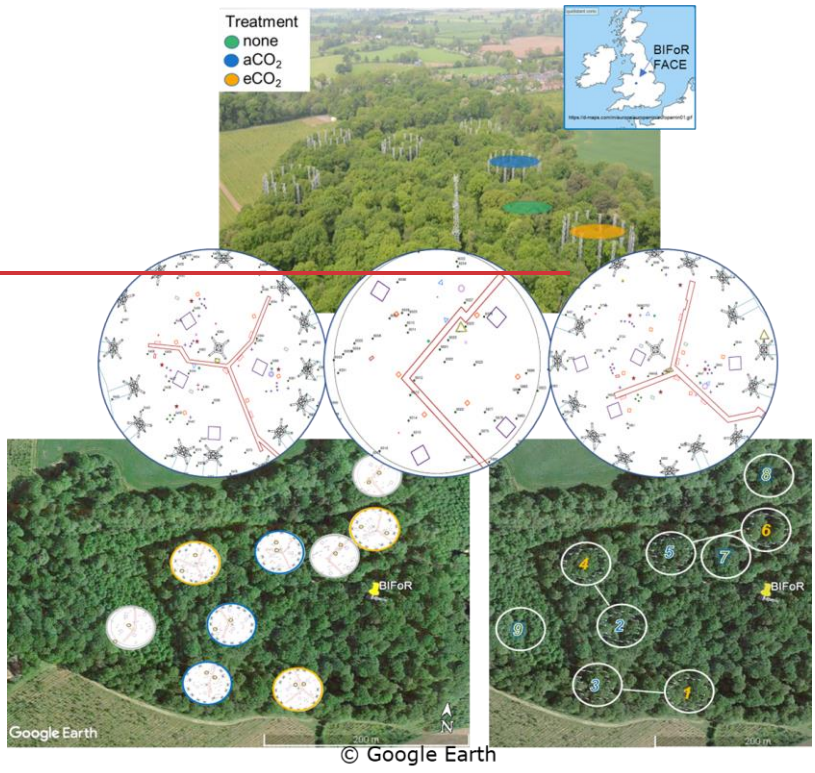

~~**Figure 1: BIFoR FACE research woods showing three treatment types and details of three arrays. Below are oak positions in all arrays. Small brown rings within arrays (lefthand picture) indicate oak trees monitored for xylem sap flow. Infrastructure treatment arrays are paired for similar soil conditions (righthand picture). Top photo image is adapted (with permission) from Ch. 7, Fig. 7 of Bradwell (2022). Top map is cropped from https://d-maps.com/m/europa/europemin/europemin01.gif**~~

The BIFoR FACE facility is in Staffordshire (52.801° N, 2.301° W), England, UK (Fig. 1). The forest is a circa 1840 plantation of oak with *Corylus avellana* (hazel) coppice. Naturally propagated *Acer pseudoplatanus* (sycamore), *Crataegus monogyna* (hawthorn), *Ilex aquafolium* (holly) and smaller numbers of woody plants of other orders (e.g. Ulmus (elm), Fraxinus (ash)) of varying ages up to circa 100 years old are also present. Some subdominant trees e.g. sycamore, hawthorn and elm, impinge on the high closed canopy. Each experimental array, circa 30 m in diameter, was selected to contain circa six live old growth oak trees. There are nine experimental arrays: three with infrastructure injecting eCO_2 (+150 µmol mol^{-1} or +150 parts per million by volume (ppmv)); three infrastructure controls injecting aCO_2 (ca. 410 to 430 µmol mol^{-1} 2017–2022); and three *Ghost* (no-treatment-no-infrastructure) controls. Data were collected for all three FACE facility treatments. Here we concentrated on oak, the dominant species, with sap flow monitoring restricted to two oaks in each of the nine experimental arrays totalling eighteen trees.

We compare individual tree's sap flux and *TWU* responses under the three treatments across the leaf-on seasons for these early experimental FACE years looking at within-year and inter-year relationships. We also describe daily, monthly and seasonal changes to sap flux and *TWU* for mature oak over five years and discuss how these results,

from our tree-centred viewpoint, will improve our understanding of future-forest water dynamics of old growth forest contributing to development of more realistic ecohydrological vegetation, soil and landscape models.

Typical experimental arrays showing target oak trees are shown in Fig. 1. Parameter symbols used in this paper are covered in Appendix A: Table A1. The term 'sap flow' is used generally when referencing heat transducer methods to measure the water movement through sapwood. Use of terms 'sap velocity' and 'sap flux' are defined in Tables A1 and A2. These usages may differ ~~to~~from other authors' usage (Lemeur et al. 2009; Poyatos et al., 2020).

.

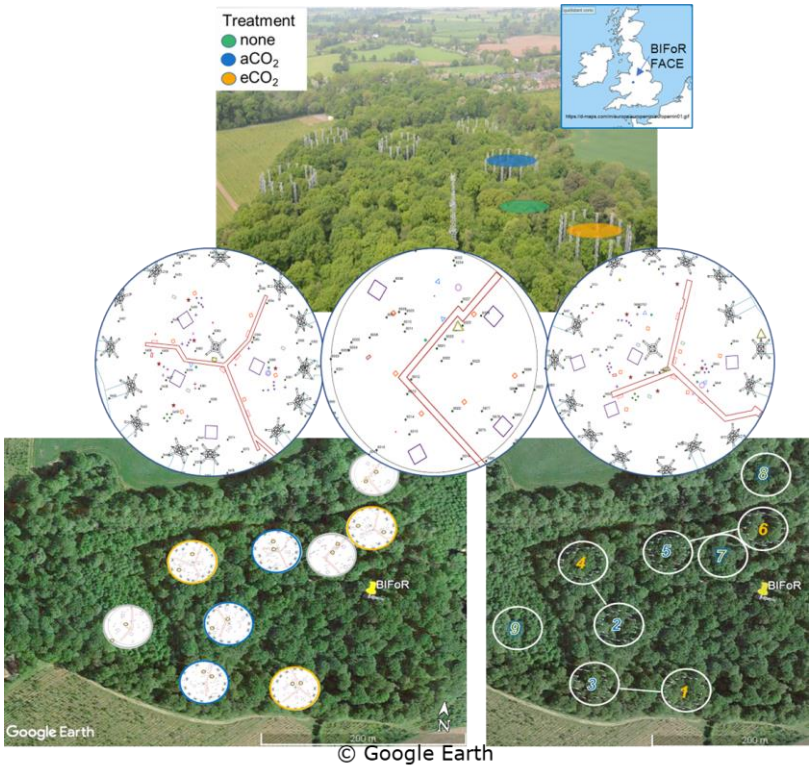

Figure 1: BIFoR FACE research woods showing three treatment types and details of three arrays. Below are oak positions in all arrays. Small brown rings within arrays (lefthand picture) indicate oak trees monitored for xylem sap flow. Infrastructure treatment arrays are paired for similar soil conditions (righthand picture). Top photo image is adapted (with permission) from Ch. 7, Fig. 7 of Bradwell (2022). Top map is cropped from https://d-maps.com/m/europa/europemin/europemin01.gif

2.2 Measurements overview

Here we report data from five treatment seasons, July 2017 to end of October 2021. The study focuses on diurnal (i.e. daylight) responses within our experimental treatment season April–October. Sap flux and *TWU* datasets for the eighteen old growth oaks are calculated from half-hourly tree stem sap flow measurements derived from HPC transducers. *TWU* data is accumulated from sap flux, then analysed monthly within the treatment season across each year. For all xylem sap flux monitored oak trees, tree identification, treatment type, array number, along with

their stem circumference and average R_b, at probeset insertion point are shown in supporting information (Table S1).

Figure S1 shows the key measurement points relating to tree hydraulics in this project. This sap flow study is supported by other core environmental (detailed below) and soil data available at our FACE experimental site (MacKenzie et al., 2021). Table S2 shows instrumentation types and related parameters used for analysis within this paper.

We experienced early leaf-on herbivory attacks on oaks by Winter moth larvae, especially in 2018 and 2019 (Roberts et al., 2022), decreasing leaf area by 20-30% and affecting the timing of canopy closure. A longer dry period occurred in the meteorological summer of 2018 (Rabbai et al., 2023), with wide variation in summer monthly precipitation across the study years. Climate during the measurement period is discussed further in the supplementary information.

2.3 Seasonal definitions

We define a plant hydraulic year, from start of the dormant season (1st November) to end of senescence (31st October). The seven months of CO_2 treatment per year (with six months of leaf-on photosynthesis) do not easily divide into standardised meteorological seasons (Spring, Summer), so we define our months of interest, including non-treatment months as shown in Table 1. The table includes two months, March to April of pre-leaf growth when oak sap starts to rise.

~~2.4~~ Season length between first leaf and full senescence/ first bare tree is relatively constant at 8 months for the years studied, although start and end vary year-on-year (Table 1). Canopy greenness, recorded as part of the PhenoCam network (https://phenocam.nau.edu/webcam/roi/millhaft/DB_1000/) shows a very rapid decline towards wintertime values from the beginning of November.~~~~Soil and throughfall precipitation data collection~~**

We have not collected phenology data specific to our target trees to capture any variability amongst individuals (see Sass-Klaassen et al., 2011).

~~Pre-treatment (2015-2017 for all arrays) and on-site soil and throughfall data were used to characterise the site. Supplementary (2018 onwards) throughfall/ soil monitoring sites were added (see Mackenzie et al. (2021)).~~ ~~Shallow soil moisture and soil temperature data were captured at least half-hourly by the same CR1000 datalogger as the sap flow data.~~

~~For plants, incident precipitation affects their function in several ways during the leaf-on season. Firstly, water droplets fall on the leaves which combined with lack of sun can prevent full photosynthesis. The canopy water mostly evaporates or may drip to ground. Secondly throughfall (P_{tf}, mm) reaching ground level may either: runoff the surface being lost to the soil, infiltrate increasing soil moisture content (providing some necessary support for root rehydration and plant water intake) or evaporate. Lastly, the soil water percolates through the saturated soil layers to replenish the water table.~~

~~Water inputs of throughfall precipitation under the oak canopy (within 2 to 3 metres of an oak stem and situated near a soil moisture monitoring position) were measured in all arrays, with Fig. S2 showing a typical installation set up.~~

Calendar months	FACE Treatment season label	Note	Oak phenology at BIFoR FACE				
			2017	2018	2019	2020	2021

March – April (*eCO₂* starts beginning April)	**Budburst & first leaf**	March is pre-treatment. **First leaf dates for** oak shown	**6 April** *	**25 April** *	**29 Mar** *	No data* (c. 6th April)	**27 April** *
May – June	**Early leaf-on**	Includes **canopy closure early leaf** of oak	-	-	-	-	-
July – August	**Mid leaf-on**		-	-	-	-	-
September – October (*eCO₂* until end October)	**Late leaf-on**	Includes **start** of senescence i.e. **first tint**	**6 Sept**	**12 Sept**	**1 Oct**	**15 Sept**	**28 Sept**
November – Feb	**Dormant**	All remaining non-treatment months	-	(after 21 Nov)**	**26 Nov****	(after 03 Nov)**	**07 Dec ****
		Assumed leaf-fall season	6 Sept 2017 to 25 April 2018	12 Sept 2018 to 29 Mar 2019	1 Oct 2019 to c. 6 April 2020	15 Sept 2020 to 27 April 2021	28 Sept 2021 to 24th April 2022

Table 1: **Definition of treatment season periods and dates for oak phenology at BIFoR FACE according to Nature's Calendar criteria for years 2017–2021 (note this excludes canopy closure data - not recorded). First tint is also recorded for year 2016 as 4th Oct. * On-site first leaf data (not obtained in 2020 due to the Covid-19 pandemic; 6th April 2020 was noted as budburst, unverified first leaf is recorded as 24th April 2020). Note: Separate records of leaf-fall season are recorded for LAI calculation purposes as Nature's Calendar data does not discriminate first leaf fall by leaf colour. ** First bare tree date recorded. Nature's Calendar link: (https://naturescalendar.woodlandtrust.org.uk/). Phenocam additionally available for all years (https://phenocam.nau.edu/webcam/roi/millhaft/DB_1000/).**

~~2.5~~2.4 FACE and meteorological measurements

Local precipitation (from a mixture of sources including Met. towers, see MacKenzie et al., (2021)) was recorded. Treatment levels of eCO_2, diurnal CO_2 treatment period, top canopy air temperature (T_a , ° C) and total solar radiation (*TG*, Watt m^{-2}), (see Figs. S8 & S10), were available from the FACE control system (Hart et al 2020; MacKenzie et al 2021). Data were averaged across the six infrastructure arrays for *TG* and T_a as the *Ghost* arrays have no FACE measurements. Set point levels of ambient CO_2 were used to control treatment application in the eCO_2 arrays (Hart et al., 2020). There are also increases in the ambient levels of CO_2 present across the years of this study of about 3.5 ppmv $year^{-1}$. ~~This alters~~The enrichment level is unique to BIFoR FACE at +150 µmol mol^{-1}, tracking the increasing ambient levels of CO_2 present across the years of this study (ca. 410 to 430 µmol mol^{-1} 2017–2022, Fig. S11) and altering the relative percentage change ~~brought about by +150 ppmv CO_2~~of $eCO_2 : aCO_2$ year on year by about 1% from 36% (beginning 2018) down to 35% (end 2021) (Fig. S11). Soil and throughfall precipitation data collection~~S11).~~

Water inputs of throughfall precipitation under the oak canopy (within 2 to 3 metres of an oak stem and situated near a soil moisture monitoring position) were measured in all arrays, with Fig. S2 showing a typical installation set-up. Pre-treatment (2015-2017 for all arrays) and on-site soil and throughfall data were used to characterise the site. Supplementary (2018 onwards) throughfall/ soil monitoring sites were added (see Mackenzie et al. (2021)). These data were captured by the same CR1000 datalogger as the sap flow data.

We have not segregated our analyses into rainy and dry days.

~~2.6~~2.5 Tree selection

~~There is variation inherent in biological individuals, in the same or different treatment types~~Variation between individuals in treatment plots can arise from their precise location within an array or from inherent (biological) variation between individuals as well as different treatments (Chave, 2013~~), which may not behave typically in~~

~~space or time.).~~ This individual-tree experiment design aims to minimise untypical variation. Accordingly the following criteria were used to select trees for sap flow monitoring:

- canopy cover completely within the array (eCO_2 & aCO_2 arrays)
- central within the plot near logger and adjacent to access facilities at height (eCO_2 & aCO_2 arrays, for sampling and porometry access)
- straight stem, preferably with little epicormic growth
- no large dead branches within the canopy which might affect the comparative biomass of the tree
- unlikely to experience seasonal standing or stream water at the base

Target oak trees for monitoring were also chosen to suit ~~the~~ physical limitations of the transducer to logger constraints rather than truly randomly.

~~2.7~~2.6 Tree characteristics

The tree size measurement approach is shown in Fig. ~~S3 and the range and mean-per-treatment values of bark circumference (metres) for all target trees are tabulated (Table S3).~~S3. All oak trees were of similar height (circa 25 m). ~~Tree stem~~Bark circumference (metres) at insertion height of probes was measured at installation (from 2017 onwards), and in subsequent winters (Jan 2020–Feb 2022). The range and mean-per-treatment values in 2022 are tabulated (Tables S1 and S3). We note that tree size will affect *TWU* (Bütikofer et al., 2020; Lavergne et al., 2020; Verstraeten et al., 2008).

Canopy spread of all target oak trees was measured around installation date (2017-2018) and repeated for all oaks in early 2022 (Fig. S3). We assume that the two-dimensional A_c, derived from the mean canopy diameter plus stem diameter, is a good approximation to actual canopy spread and hence the whole canopy surface experiencing leaf transpiration. For trees of similar height we assume that allometric shape to estimate whole canopy volume will be similar. On the second occasion in 2022 we measured the asymmetry of each tree stem across the probeset cardinal positions (East-West) and right-angles to this (North-South) as a check of mean R_b value for sap flux calculations.

~~Short incremental wood cores (circa 10 cm long, 4 mm diameter) were taken from two old growth oaks outside of the experimental arrays. Microcores were also taken near all 36 target oak probeset installation positions. These cores were used to determine wood hydraulic properties (Edwards and Warwick, 1984; Marshall, 1958) for sap flux calculations (see also stage 4, Table A2 and definitions Table A1). In summer 2021 woodcores taken from some of the target oaks were further analysed to check the conversion (xylem woody matrix) factors from heat velocity to sap velocity and to verify the active xylem radial width. The visibly active xylem (sapwood) is typically between seven and 50 mm when viewed in wet cores. The uncertainty in heartwood boundary H (m), as described in Appendix B, could be resolved in future similar studies by taking short cores prior to installing instrumentation.~~

~~2.8~~2.7 Xylem sap flux

Details of the xylem sap flux measurement method and associated calculations are provided in Table A2 and Appendix C. Each target oak tree had two probesets, East and West facing (Fig. 2). Appendix B discusses the limitations which the time-out characteristic places on this set of HPC data and consequent results. Validity of high value extrema is considered within our analysis.

To determine whole tree sap flux several tree characteristics were used: (a) tree stem circumference at insertion point, (b) bark thickness~~, from which~~. From these data we derived tree stem cambium radius at insertion point (R

(, m) and subsequently heartwood radius (*H* (, m) from sensor spacing. *H* (m) could not be determined from 10 cm cores as these were not taken for all sap trees monitored.

The xylem sap flow installations in target trees commenced in Jan. 2017. All *Ghost* oak trees provided data from August 2017 and commissioning of all 18 oak trees was completed by autumn 2018. All oak sap flow installations were successful and a total of 12,259 days of individual tree data (770,667 diurnal sap flux measurements across all months) were processed for the 2017–2021 *TWU* analysis. Resulting data gaps in the earliest installations affected four of the 36 probesets installed in four trees August 2017 until September 2019.

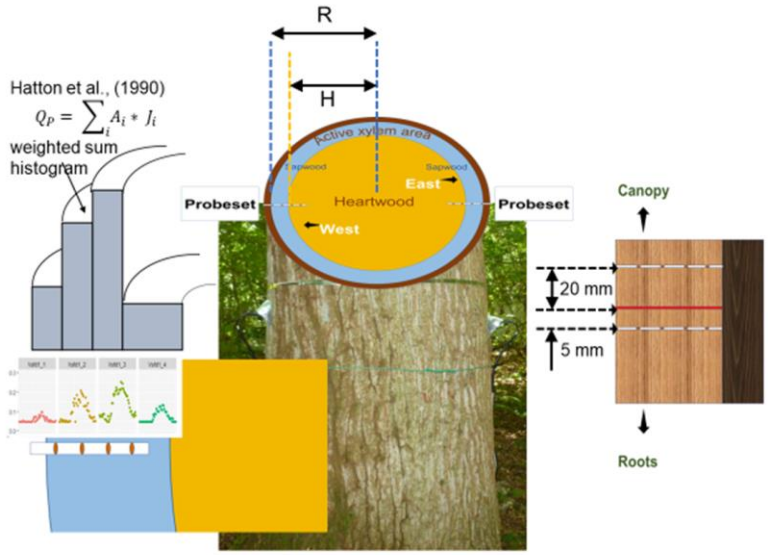

Figure 2: Showing sap probeset layout, spacing dimensions between probes and indicative illustration of Hatton et al., (1990) weighted sum histogram, where R (m) is the radius to the cambium and H (m) is the heartwood estimated radius, both at the probeset insertion height. All equations and variables also defined in Tables A1 and A2. Graphical insert is Fig. C1(b).

2.8.1 In respect of quality assurance of raw HPC data

commissioning and failure data were recorded for each probeset. This enabled a combination of data file amendment (especially for the earliest installations on separate loggers) and post capture filtering to eliminate periods of invalid data for each probeset.

2.8.21.1.1 Heat pulse to xylem sap flux calculations.

Figure C1 shows example positional (i.e. thermocouple-specific), point sap flux density data from four probesets in two trees.Sap flux and Note the increase in sap flux density towards the centre of the sapwood, decreasing again towards the heartwood (Fig. C1(b)).

~~2.8.3 Converting point xylem sap flux data to~~ whole tree water usage.

Using ~~tree~~ cambium radius (*R*) data, estimated heartwood radius (*H)* (0.05 m smaller than the inner sensor radial position), along with transducer radius positions (r_z), ~~point sap flux density is converted to~~ volumetric (half tree) total sap flux ~~by using the integration of the point sap fluxes over the active sapwood conducting area. Output from this stage (Stage 5, Appendix Table A2 and Appendix C) gives a combined sap fluxis~~ calculated for each probeset (Fig. 3).

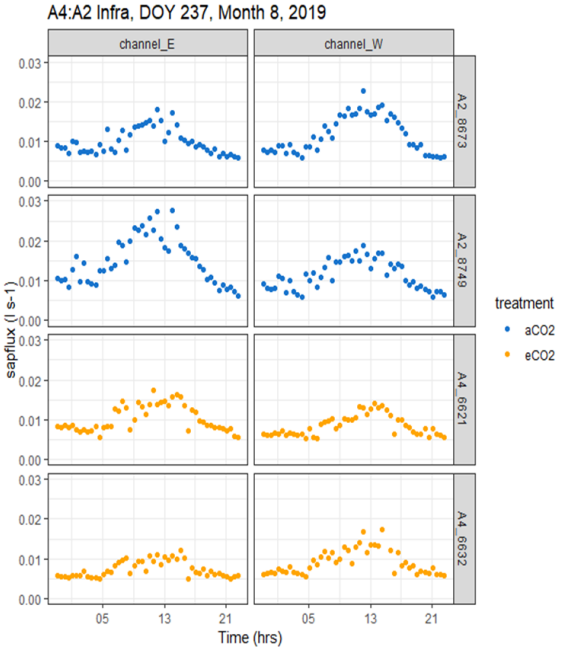

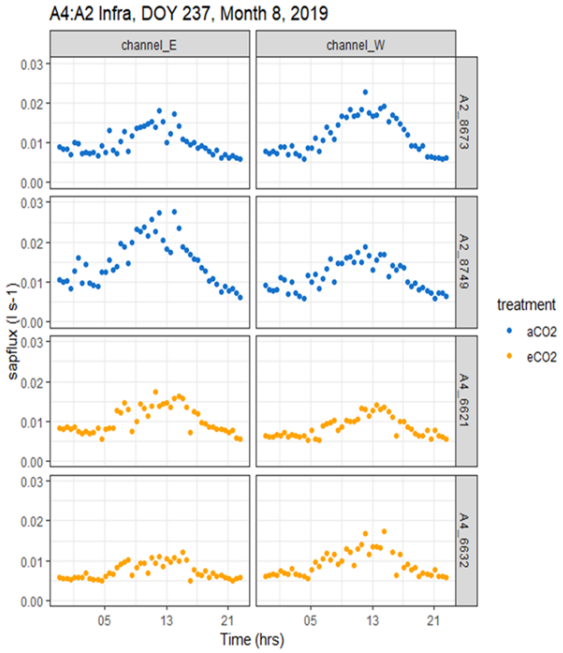

Figure 3: An example data visualisation from a sunny August day in 2019 showing output of Stage 5 combined point sap flux (litres s^{-1}) for four infrastructure trees with E facing (left) and W facing (right) probesets working: Array 4 (eCO_2), at top and A2 (aCO_2), at bottom. Time is in UTC.

Example diel sap flux patterns for the *Ghost* arrays in August 2019 (before filtering to eliminate nocturnal data) are shown in Fig. ~~4(a) as an example, for the *Ghost* arrays~~4(a), with East– and West–facing probesets in each column. The sap flux data still show minimum threshold levels (which vary by tree size) determined by the post–heat–pulse sampling period. It is noticeable that there is often circumferential imbalance in xylem sap flux in the East (lefthand column of Fig. 4(a)) and West (righthand column of Fig. 4(a)) probeset position data, which reflect the asymmetry in growth ring width around the stem typical in these old growth trees. The blank panels represent faulty probes (in two *Ghost* trees~~)~~), which were corrected by autumn 2019.

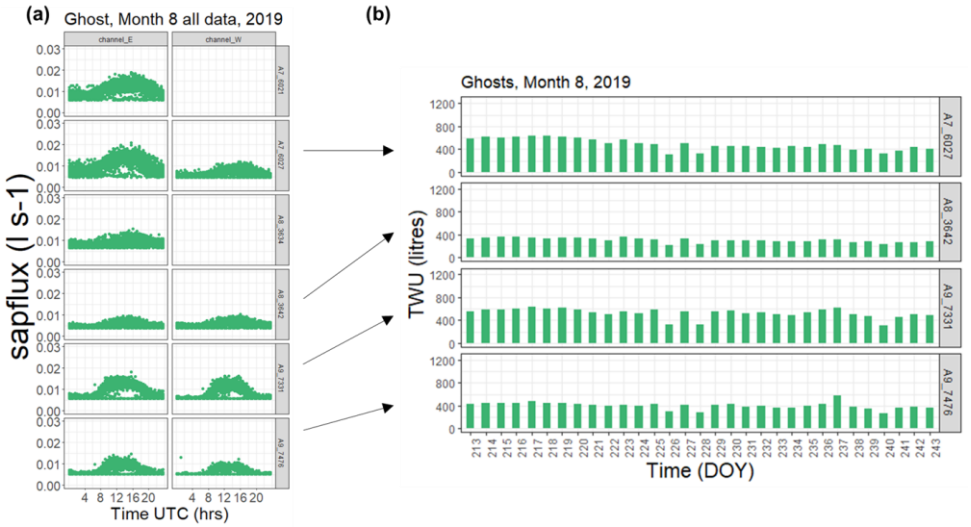

Figure 4: Example *Ghost* Array xylem sap responses in August 2019. (a) diel (24hour) tree sap flux for all days in August 2019 are superimposed. E (left) and W (right) facing probesets for six *Ghost* trees show circumferential imbalance in xylem flux. All data for the individual month is superimposed across time-of-day sampling (hours, UTC). Frequency of sampling is every 0.5 hrs. Faulty probeset positions are shown blank. (b) Example of accumulative daily diurnal water usage (*TWU*) per tree totalled for E and W facing probesets across month 8 2019 for four *Ghost* trees having both E and W probesets functioning with the other two *Ghost* trees omitted due to faulty probesets. Time is day-of-year (DOY.).

To compare individual tree responses across the leaf-on seasons~~, further data filtering is required.~~ we filter the half-tree sap flux parameters using the solar azimuth and solar radiation parameters captured from the FACE control instrumentation (solar azimuth > -6~~°~~,° and solar radiation > 0 W m^{-2}) to give just daylight (diurnal) data. Where both probesets in a tree are providing good data, a mean whole tree sap flux is ~~then~~ derived and accumulated into *TWU* (Fig. 4(b~~)) as)~~). We had sufficient whole-tree data to ~~not include results where probesets had failed. In future analysis we could use half-tree data once we understand the proportion of sap flux and *TWU* exhibited by each~~exclude single probeset ~~(e.g. following failure of contact with sapwood of a previously functioning probeset).~~results.

There are day-to-day differences in *TWU* between trees in our study (e.g., Fig. 4(b)) even though all of them experience very similar environmental conditions and this pattern is replicated across the three treatment types. The *TWU* data reported here compare well to results from other studies (Table S4: David et al., 2013; Sánchez-Pérez et al., 2008; Tatarinov et al., 2005; Baldocchi et al., 2001).

~~2.9~~2.8 Data processing, visualization and analysis

Manually collected data was pre-processed as .csv files for import to 'R'. Raw data from dataloggers were processed, visualised and consequently analysed using 'R' versions 3.6.2, 4.0.3 and 4.2.1 (R Core Team, 2020, 2021 and 2022), R Studio (RStudio Team, 2022) on Windows 10 x 64 (build 1909). ~~All~~Results figures were created using R package *ggplot* (Wickham, 2016). Other standard packages (e.g. *lubridate*) are listed in R scripts. Regressions between R_b and water usage, and between R_b and A_c were calculated using the *lm* function. Box and whisker plots to visualise seasonal and monthly differences in sap flux and water usage between trees and treatments were generated in *ggplot* where standard Tukey (McGill et al., 1978) percentiles (median + interquartile range) whiskers (1.5 * IQR from each hinge, where IQR is the inter-quartile range) plus points for outliers are used.

~~We used~~ LOESS (locally estimated scatterplot smoothing) was used for exploratory analysis of the time series data (e.g. Fig. S12), an approach that, does not rely on specific assumptions about the distributions from which observations are drawn. Levene tests (Levene, 1960) were carried out using *leveneTest* from the *car* library. ANOVA models to test hypotheses used the functions *anova* and *summary*. Function *autoplot* from the *ggfortify* library was used to test the assumptions of normality of the residuals.

3 Results and Discussion

This section is organised as follows: We first report general characteristics of the distribution of sap flux (Section 3.1) and then develop relationships between *TWU*, R_b, and projected canopy area, A_c. (Section 3.2). Subsequently we discuss the characteristics of TWU_n (litres d^{-1} mm^{-1}, Section 3.3), which we use to test for treatment effects in an analysis of variance (Section 3.4). We examine eCO_2 and infrastructure treatment effects (Section 3.5), and finish with a brief assessment of limitations to the approaches adopted (Section 3.6). We discuss the effects of seasonal weather in the supplement Appendix A.

3.1 Sap flux within the season and between years.

Diurnal stem sap flux responses to canopy photosynthetic demand typically exhibit increased sap flux from dawn to around midday (UTC ~ local solar time at the site) with an approximately symmetrical decrease to dusk (Figs. 3 & 4). Exploring these data illustrates some of the important characteristics of this sap measurement approach. Figure 5 shows diurnal sap flux (i.e. Q_E and/or Q_W, data derived from each probeset, East- and West-facing, installed per tree) in each of three *Ghost* array oaks (selected for smallest, largest and medium sized stem see Tables S1 and S3) for treatment seasons 2018–2021. The partial year 2017 is not shown. We have retained Q_E and Q_W to show more of the short-term variability rather than averaging to Q_T, as single probeset results demonstrate circumferential imbalance (Fig. 3 & Fig. 4(a)) which can change with year of operation (Fig. S4).

Interquartile ranges are generally larger in the middle of the growing season for all sizes of example trees and collapse towards the minimum detectable value for each tree size at either end of the growing season. The minimum detectable sap flux using the present method is tree-size dependent (Appendix A2, Stage 5): 0.0035 litres s^{-1} (3.5 ml s^{-1}), for the smallest tree in Fig 5; 5.2 ml s^{-1} for the medium-sized tree; and 6.5 ml s^{-1} for the largest tree shown. The imbalance between the probeset data on the example trees (Fig. 5) can be up to +/-25% (Fig. S4). This is greater in the earlier years 2017 and 2018. ~~–~~This imbalance determines the spread of the IQR when normalised tree values are combined. All the large tree example sap flux values lie within a factor of three of the minimum detectable value (i.e. to 0.02 litres s^{-1}) until June 2020 (more than four years after installation) after which ~~slightly more~~larger extreme ~~outlier ranges exist~~values are present.

The distributions of the three examples are clearly offset by tree stem size, suggesting that normalisation by this measure may be useful for inter-tree comparison (section 3.3). For these example trees, mean monthly diurnal sap flux ~~increases~~increased in the spring from first leaf (see phenology in Table 1, above) to achieve peak values in July in 2018 and 2021. In 2019 and 2020, increases in mean monthly diurnal sap flux were more gradual through the treatment season, reaching peak values in August (2019) and September (2020). There was then a faster decrease in sap flux to end of October (the end of the CO_2 treatment season) or later, presumably due to leaf senescence and the shortening of daylength.

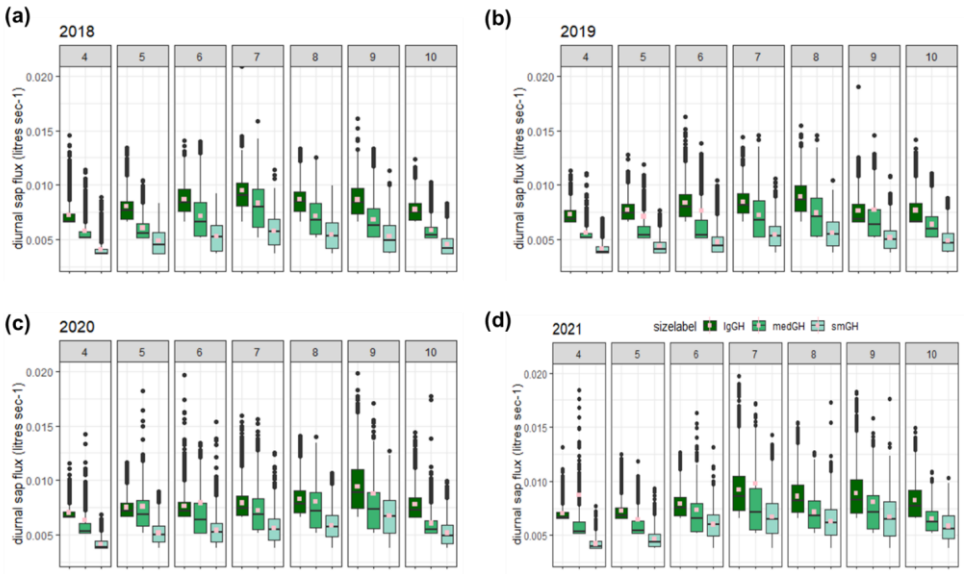

Figure 5: Comparison of diurnal sap flux measured in each probeset for three (small, medium and large) *Ghost* (no-infrastructure control) trees in years 2018- 2021, panels (a), (b), (c), and (d), respectively, across the treatment season April–October. Monthly 95%ile values are shown separately (Supplement Fig. S5). The graphical display is cropped at a sap flux of 0.02 litres s^{-1}. The distributions are shown as box and whisker plots showing median and interquartile range (IQR, 25%ile to 75%ile) with whiskers calculated as 1.5 x IQR from the hinge and points for outliers. Mean values, calculated from the entire range of data, are shown as spot (pink).

It is evident there are highly skewed distributions in Fig. 5. Figure S5 reports 95%ile sap flux values for each probeset and month across 2017-2021, showing variability in the timing of highest monthly 95%ile sap flux between half-tree data for each tree across the years of study. 95%ile sap flux is not synchronised for all probesets on a monthly basis, indicating the dominant role of individual tree characteristics or position in determining sap flux extrema (Dragoni et al., 2009). Although minimised as much as practicable (see 2.6, above), such individual characteristics ~~may~~cannot be ~~related~~completely eliminated and relate to major changes in branch structure (e.g., from wind damage or mortality) affecting canopy photosynthetic controls. They may also depend on the aspect of the tree and competition for root water (proximity to other trees), indicating seasonal influences on leaf, branch and root growth.

3.2 Diurnal *TWU* variation between trees.

3.2.1 *TWU* as a function of bark radius

Example relationships between R_b, (mm) and monthly mean *TWU* (*TWU*, litres d^{-1} $month^{-1}$) for all trees with both probesets working were first analysed for 2019 summer months. July was used for comparison as typically it exhibits maximum *TWU*. The hypothesis that *TWU* is a function of R_b was tested by a simple regression model. The best fit model for the combined 2019 data across all treatments was a simple linear fit; quadratic fits were tested and rejected. During July 2019, due to two probesets malfunctioning, *Ghost* tree *TWU* results did not include trees as large as the largest in the infrastructure arrays as explained in Methods above. Data from six, 13, 17 or 17 trees were used for years 2018, 2019, 2020 & 2021 respectively.

	slope	SE	R^2	Adj. R^2	intercept	t	df	p
	(litres per day per millimetre)				(litres)			
Jul-18	3.716	0.742	0.86	0.83	-721	5.011	5	p<0.01
Jul-19	3.268	0.442	0.82	0.81	-621	7.399	12	p<0.001
Jul-20	2.233	0.511	0.54	0.52	-286	4.370	16	p<0.001
Jul-21	2.967	0.654	0.58	0.55	-476	4.537	16	p<0.001
Aug-19	2.913	0.310	0.88	0.87	-552	9.391	12	p<0.001
July 2017-2021	3.100	0.422	0.50	0.49	-545	7.340	54	p<0.001

Table 2: Linear regression model parameters for July mean *TWU* (*TWU*, litres d^{-1} $month^{-1}$) versus bark radius at insertion point (R_b, mm). August 2019 is also shown. Final row shows model statistics for July all years 2017-2021, for 55 trees. The table does not discriminate *TWU* in respect of treatment. Statistical results are rounded to four significant figures accounting for some uncertainty. See Appendix A Table A1 for statistical abbreviations.

Inserted Cells

Inserted Cells

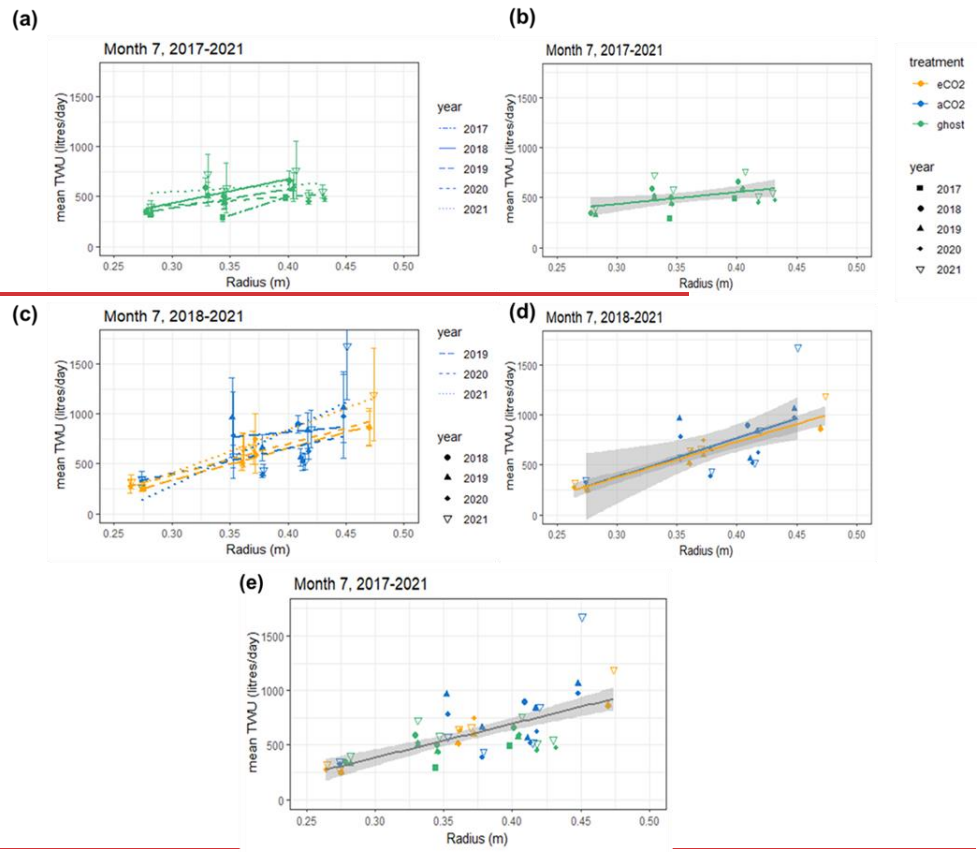
(a)
Month 7, 2017-2021
mean TVMJ (litres/day)
Radius (m)
year
2017
2018
2019
2020
2021
(b)
Month 7, 2017-2021
mean TVMJ (litres/day)
Radius (m)
treatment
eCO2
aCO2
ghost
year
2017
2018
2019
2020
2021
(c)
Month 7, 2018-2021
mean TVMJ (litres/day)
Radius (m)
year
2019
2020
2021
year
2018
2019
2020
2021
(d)
Month 7, 2018-2021
mean TVMJ (litres/day)
Radius (m)
(e)
Month 7, 2017-2021
mean TVMJ (litres/day)
Radius (m)

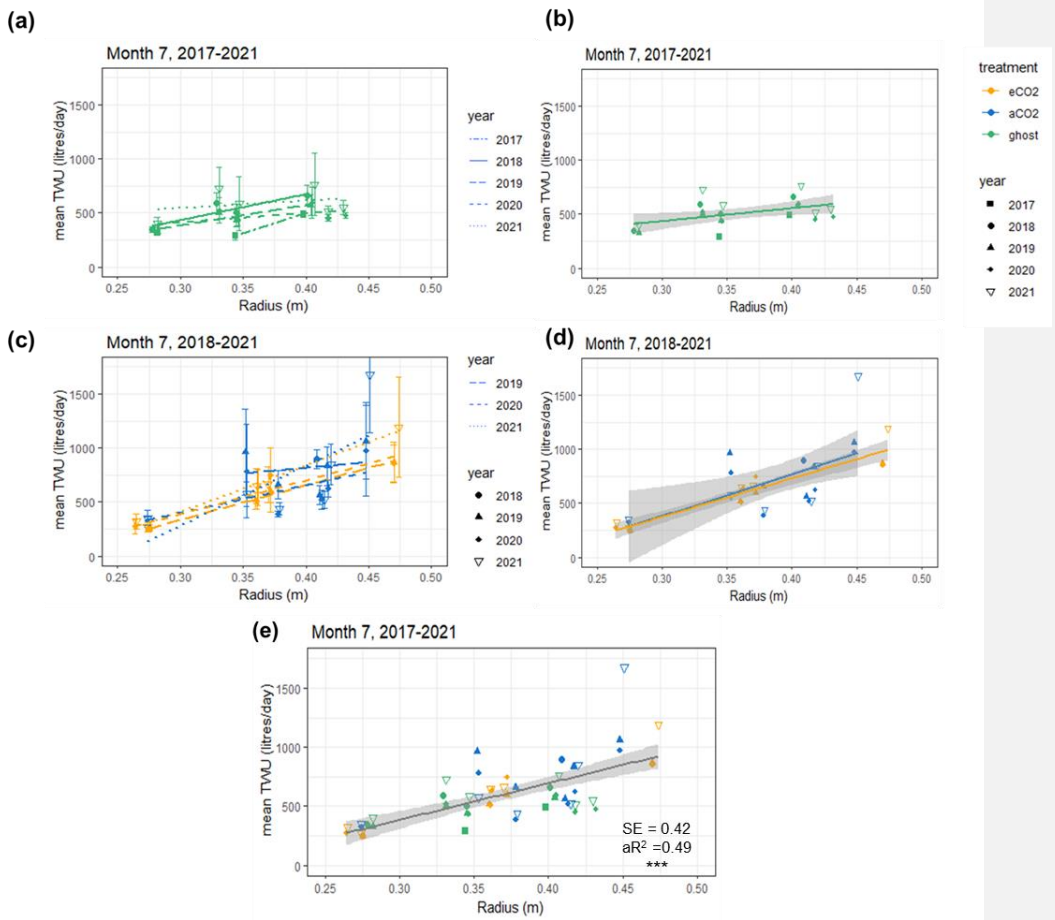

Figure 6: Mean July *TWU* (*TWU*, litres d^{-1} $month^{-1}$) versus bark radius R_b (m) at measurement height is shown for the three treatment types in years 2017–2021. (a), (b) show *Ghost* (no-infrastructure-no-treatment) trees all years. (c), (d) show infrastructure arrays for treatment (eCO_2) and infrastructure control (aCO_2), years 2018–2021. (b) and (d) show treatment regression lines for all years combined, (e) shows points for all years with single regression line. R_b is linearly proportional to *TWU* (mean slope 3.1 ± 0.4 litres d^{-1} mm^{-1}) . (a) and (c) error bars show sd. (e) additionally shows significance (* p<0.001), SE and adjusted R^2 (aR^2) values.**

All years 2017–2021 of July data are shown in Fig. 6, illustrating the differences by year (Table 2) and treatment. The shorter regression for the *Ghost* array trees (Fig. 6(a) and (b)) has a smaller slope than infrastructure (eCO_2 and aCO_2) array trees which exhibit similar slopes. Table 2 lists July model slopes for years 2018–2021 all treatments combined. The slopes are within +20%, -30%, giving a mean slope of 3.1 ± 0.4 litres d^{-1} mm^{-1}, although the steepest slope (July 2018) and the shallowest slope (July 2020) differ by more than their combined standard errors and so may represent different relationships. The intercept of the linear regression is not physically meaningful as we are only considering a relationship for trees of R_b between 0.25 and 0.5 m. The results confirm the recent study by Schoppach et al., (2021) (and supporting reference (Hassler et al., 2018)) in respect of the relationship between DBH and the water usage of oak.

The slopes of the three treatments in July for all years' data were also compared to determine differences due to treatment (Table S5). There is 10% difference between infrastructure treatment trees' slopes (Table S5 and Fig.

6(d): aCO_2 slope = 3.86, SE = 1.25 litres d^{-1} mm^{-1}; eCO_2 slope = 3.55, SE = 0.31 litres d^{-1} mm^{-1}), which is not statistically significant given the standard error on the slopes. Overall, for infrastructure treatment trees (eCO_2 and aCO_2; Fig. 6(d)), the slope is greater than for no-infrastructure *Ghost* array trees (slope = 1.2, SE = 0.47 litres d^{-1} mm^{-1}) (Fig. 6(b)) and the magnitude of ***TWU*** for all infrastructure trees is greater for a given size.

3.2.2 Factors affecting ***TWU*** as a function of R_b

The relationship with ***TWU*** varies on a year-by-year basis between 2.2 and 3.7 litres per day per millimetre of R_b. This is due, in years of lower values, to relatively larger decreases in ***TWU*** by large trees compared to the smaller trees in the sample. Oaks respond sub-daily to solar radiation reduction events (Fig. S8) during cloud cover, suggesting that the year-to-year differences in slope (Table 2) are affected primarily by environmental factors (Wehr et al., 2017). In July 2020, the wettest year for mid-leaf (see Table ~~6~~S9 and Figs. 10 and 12 below), we are not able to distinguish whether the smaller slope arises from (a) smaller trees' ***TWU*** being enhanced due to the truncation effect (Appendix B) or (b) larger trees' ***TWU*** being suppressed under poor light levels relatively more than the smaller trees, or (c) a combination of these two factors. Nonetheless, the inter-year variation in the regression is likely due to monthly weather variation, such as different numbers of days of full sunlight or more days of rain (Table ~~6~~S9 and Fig. ~~12~~S15) but this remains to be tested.

3.2.3 Canopy area A_c as a function of bark radius, R_b.

Canopy area, A_c (m^2), measured in year of installation ('First') and early 2022 ('Last'), correlates closely with R_b (Fig. 7 and Table 3, also Table S6 for data concerning repeat measures for each tree). On average, A_c is linearly proportional to R_b (ca. 617 ± 108 m^2 m^{-1}; $0.261\ m \leq R_b \leq 0.473\ m$). There are changes in A_c (some positive and some negative) between first and last measurements.

The three treatments do not show statistically significant differences in A_c per unit tree radius; eCO_2 has the greatest A_c per R_b but the other fits, although smaller in the mean slope are fitted much less well to the linear model, resulting in much larger standard errors on the mean slope (Table 3, column 2).

The measurements of A_c taken here are useful to assess water usage per unit of projected area of plant canopy but are insufficiently precise to quantify treatment effects. Changes in A_c, presumably due to a combination of measurement uncertainties and other influences such as branch growth, or loss during severe wind events, do not impact on the significance of the overall A_c versus R_b relationship (Table 3, all points).

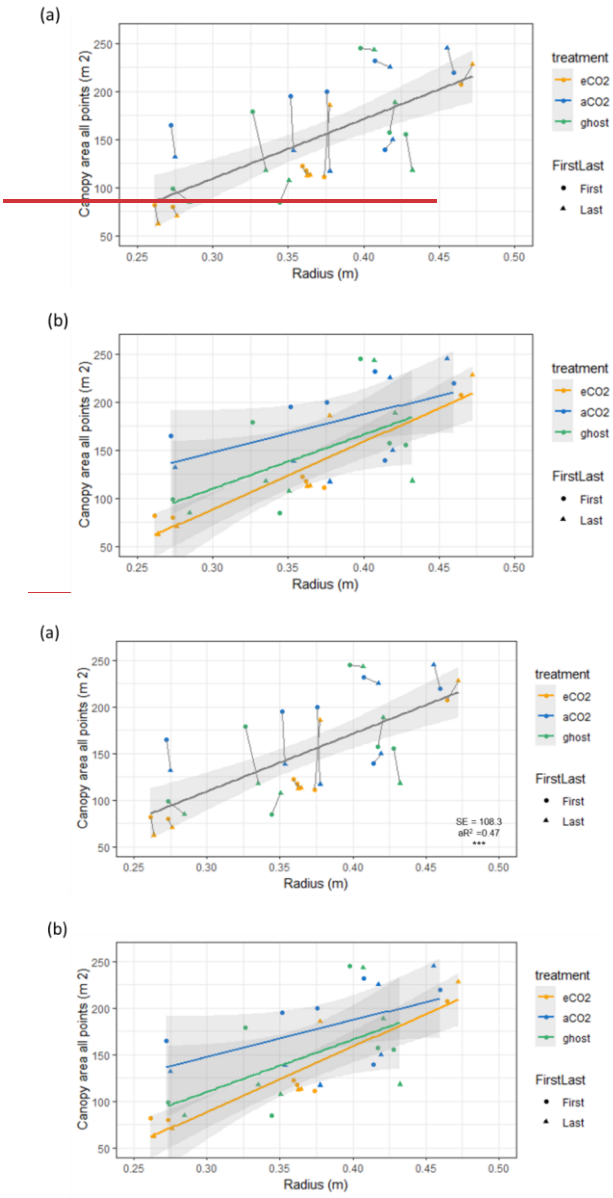

Figure 7: Canopy area A_c (m^2) variation with bark radius R_b (m) for target oak trees measured in dormant season on two occasions per tree. Significance values, SE, adjusted R^2 (aR^2) and slopes are shown in Table 3.First measurement year is 2017-2018. Last measurement year is 2022. (a) shows a linear model for all trees monitored. showing significance (* signifying p<0.001), SE and aR^2 values. A_c is linearly proportional to R_b (ca. 617 ± 108 m^2 m^{-1}; 0.261 m ≤ R_b ≤ 0.473 m). A line joins first and last measurements. (b) shows linear model relationships by treatment. Error bars show sd.**

	slope	SE	R^2	Adj. R^2	intercept	t	Df	p
	$m^2\ m^{-1}$				(m^2)			
2017-2022 canopy area aCO_2	391	195.1			30.50	2.00	10	0.073
2017-2022 canopy area eCO_2	698	30.44			-120.7	7.72	10	p<0.001
2017-2022 canopy area *Ghost*	560	263.0			-58.16	2.14	10	0.059
2017-2022 all points	617	108.3	0.49	0.47	-75.54	5.69	34	p<0.001

Inserted Cells

Inserted Cells

Table 3: Oak tree canopy area A_c (m^2) versus bark radius (m) at insertion point. Data from 18 trees for two (first, last) A_c measurements are shown (4^{th} row) and modelled by treatment (rows one to three). First readings soon after installation, last readings in early 2022. Statistical results are rounded to four significant figures accounting for some uncertainty.

We could use either R_b or A_c to remove the tree size-dependence of sap flux (Fig. 5) and hence *TWU*, exemplified in Fig. 6 above. Using the overall regressions in Tables 2 and 3, along with measurement error, the average July diurnal water usage is 5 ± 0.3 litres $d^{-1}\ m^{-2}$ of A_c. We use R_b (Fig. 8) below as the more convenient normalising factor (as it can be measured manually more easily and accurately by forest practitioners).

3.3 Yearly and seasonal variation of *TWU*.

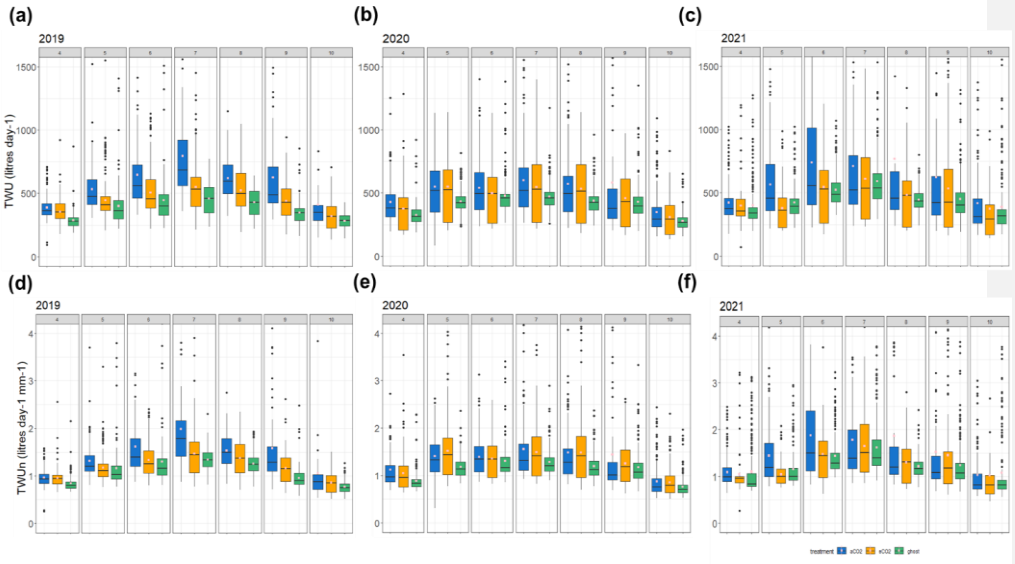

Figure 8: Treatment comparison of *TWU*. For years 2019- 2021 the *TWU* data is shown for the three treatment types. Tree data are combined for each treatment month April–October. The distributions are shown as box and whisker plots showing median and interquartile range (IQR, 25%ile to 75%ile) with whiskers calculated as 1.5 x IQR from the hinge and points for outliers. Mean values, calculated from the entire range of data, are shown as spots (pink). Panels (a), (b), and (c) show *TWU* (litres d^{-1}) for years 2019, 2020, 2021. Panels (d), (e), and (f) show TWU_n (litres $d^{-1}\ mm^{-1}$), i.e. *TWU* normalised by bark radius (mm) at stem probe insertion height.

Box and whisker plots show *TWU* (Fig. 8(a), (b) and (c)) for years 2019–2021 and treatments across the treatment season (April–October). In comparison, *TWU* normalised by individual tree bark radius R_b, which we will call TWU_n (litres d^{-1}, mm^{-1}) is shown for the same years in Fig. 8(d), (e) and (f). Years 2017 and 2018 are omitted because they have fewer data (Fig. S6) and are not fully representative of the tree size range across treatments.

For years 2019–2021 (Fig. 8(a),(b),(c)), mean, median and 75%ile *TWU*s (litres d^{-1}) increase steadily with daylength and solar radiation (Fig. S8) from around budburst (April/ May) to a broad summer maximum (June, July, August), and then decline with daylength to full leaf senescence (October−November). Similar patterns are exhibited during 2017 and 2018 (Fig. S6).

In comparison, TWU_n exhibits lower within-month variability indicated by smaller interquartile ranges, though the basic relationship between treatments remains (Fig. 8(d), Fig. 8(e) and Fig. 8(f)). There is close correspondence in *TWU* and TWU_n inter-year patterns for all three treatments across the leaf-on seasons. The starting levels in April (lowest 2019) and peak month (July or August) of median TWU_n vary year-on-year, likely resulting from differing throughfall and soil moisture retention within the previous 12 months (~~section 3.5, below).~~supplement Appendix A).

Figure S7 shows the monthly sap flux and TWU_n 95%iles for all trees illustrating the variation of high value extrema.

3.4 ANOVA testing of hypotheses.

Variance of tree water usage is tested using normalised data (TWU_n) per tree grouped by treatment type (Fig. 9, Table 4 and Table 5). Mean values for TWU_n in treatment season and July, for each of the years 2019 to 2021, are calculated and compared. Levene's test was applied showing heterogeneity of variance of TWU_n data for each model using both the median and the mean. The results are reported in Table S7 for infrastructure groups (eCO_2 and aCO_2) and Table S8 for control groups (aCO_2 and *Ghost*). Additional analyses were undertaken: ANOVA using the ~~ln-~~natural logarithm transform and the non-parametric Wilcoxon ranked-sum test. Both produced very similar results to the ANOVAs reported here.

Hypothesis 1 concerning the effect of CO_2 is tested by one-way ANOVA between eCO_2 TWU_n compared with aCO_2 TWU_n (Table 4, Fig. 9). ~~The enrichment level is unique to BIFoR FACE at +150 µmol mol^{-1}, tracking the increasing ambient levels of CO_2 present across the years of this study (ca. 410 to 430 µmol mol^{-1} 2017–2022, Fig. S11) and altering the relative percentage change of eCO_2: aCO_2 year on year.~~

In 2019 and 2021 seasons, the ANOVA suggested a highly significant ($p<0.001$), -19% to -13.9%, reduction in eCO_2 TWU_n compared with aCO_2 TWU_n (Fig. ~~99 blue-yellow comparisons~~, Table 4). In 2020, ~~a marginal effect~~the 3% reduction was marginally significant ($p=0.08$) for eCO_2 TWU_n vs. aCO_2 TWU_n ~~was found: -3% (p=0.08).~~. For

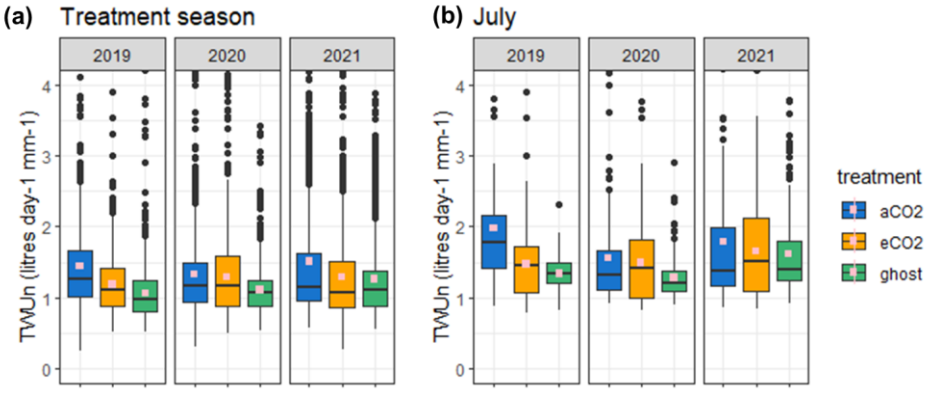

July-only results, the ANOVA suggested a highly significant (p<0.001) -26% reduction in eCO_2 TWU_n compared with aCO_2 TWU_n in July 2019, whilst comparisons for July 2020 and July 2021 showed no significant differences (Fig. 99 blue-yellow comparisons, Table 4).

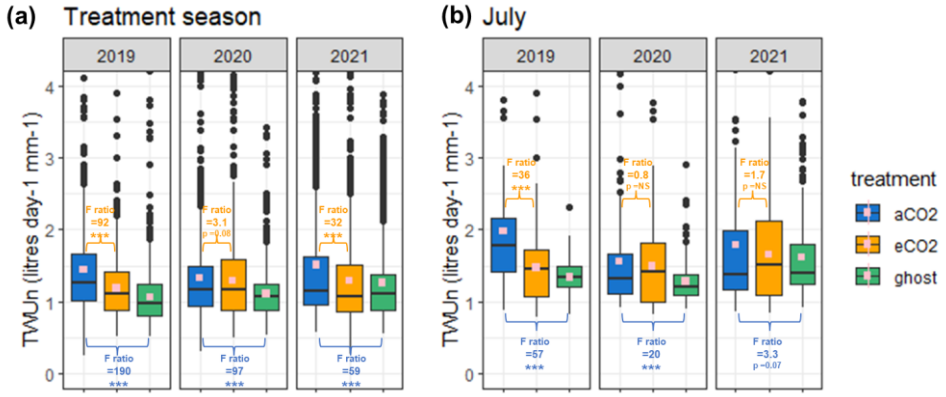

Figure 9: Treatment comparison of *TWU*. For years 2019- 2021 the ~~*TWU*n~~*TWU*n (litres d^{-1} mm^{-1}) data is shown for the three treatment types. (a) The season data April–October is combined for each year. (b) July for each year is shown. The distributions are shown as box and whisker plots showing median and interquartile range (IQR, 25%ile to 75%ile) with whiskers calculated as 1.5 x IQR from the hinge and points for outliers. Mean values, calculated from the entire range of data i.e. season (a) or July (b) are shown as spots (pink). p-values and F ratios are indicated in orange (hypothesis 1, Table 4) for *eCO₂: aCO₂* one-way ANOVA model and blue (hypothesis 2, Table 5) for *aCO₂: Ghost* one-way ANOVA model. Values for both treatment season (a) and July mean (b) *TWU*n in each year are given. Tables ~~4 and 5~~also give ~~the p values, F ratio and~~ % differences of both treatment season and July mean *TWU*n ~~in each year against the hypotheses (Table 4 for hypothesis 1 and Table 5 for hypothesis 2) using one-way ANOVA.~~ .

	2019 p value	2019 F ratio	2019 %	2020 p value	2020 F ratio		2020 %	2021 p value	2021 F ratio	2021 %
Season	**< 0.001**	**91.90**	**-19%**	p>0.05, actual value 0.079	3.09		-3%	**<0.001**	**32.27**	**-13.9%**
July only	**< 0.001**	**35.61**	**-26%**	p>0.05, actual value 0.37	0.80		-4.5%	p>0.05, actual value 0.19	1.71	-7.3%

Table 4: Hypothesis 1 CO_2 effects. One-way ANOVA p-value, F ratio, and % difference summary for mean *eCO₂ TWU*n, compared with mean *aCO₂ TWU*n, in years 2019-2021. Mean values are compared, calculated from the entire range of data for season data April–October (Fig. 9(a)) and July (Fig. 9b), for each year as shown. Bold typeface indicates p-value <0.05.

Hypothesis 2 concerning the effect of infrastructure is tested by one-way ANOVA between mean values of aCO_2 TWU_n compared with *Ghost* TWU_n (Table 5, Fig. 9~~).~~ blue-green comparisons). For all 2019, 2020 and 2021 seasons, the ANOVA suggested a highly significant (p<0.001) 37% to 20% increase in aCO_2 TWU_n compared with *Ghost* TWU_n (Fig. 9, Table 5). For July-only TWU_n, the ANOVA suggested a highly significant (p<0.001) 48% to 22% increase in mean aCO_2 TWU_n compared with *Ghost* TWU_n for July 2019 and July 2020 (Fig. 9, Table 5). For July 2021, a marginal 10% effect for aCO_2 TWU_n vs. *Ghost* TWU_n was found~~: 10%~~ (p=0.07).

	2019 p value	2019 F ratio	2019 %	2020 p value	2020 F ratio	2020 %	2021 p value	2021 F ratio	2021 %
Season	**< 0.001**	**187.38**	**+37%**	**< 0.001**	**96.66**	**+20%**	**<0.001**	**58.81**	**+20%**
July only	**< 0.001**	**57.35**	**+48%**	**< 0.001**	**19.95**	**+22%**	p>0.05, actual value 0.071	3.29	+9.9%

Table 5: Hypothesis 2 infrastructure effects. One way ANOVA p-value, F ratio, and % difference summary for aCO_2 compared with *Ghost* TWU_n in years 2019-2021. Mean values are compared, calculated from the entire range of data

Inserted Cells

for season data April–October (Fig. 9(a)) and July (Fig. 9b) for each year as shown. Bold typeface indicates p-value <0.05.

3.5 Seasonal weather and phenology

3.5.1 Effects of phenology and precipitation on deciduous tree water usage

Season length between first leaf and full senescence/ first bare tree (growing season) is relatively constant at 8 months for the years studied, although first leaf varies year-on-year (Table 1). We have not collected phenology data specific to our target trees to capture any variability amongst individuals (see Sass-Klaassen et al., 2011). We define a plant hydraulic year, from start of the dormant season (1st November) to end of senescence (31st October). Local reference precipitation (P_r, mm) for the period of interest (November 2015 to December 2021) in both the meteorological year and the tree hydraulic year averages to approximately 748 mm yr^{-1} (Table 6). Table 6 reports Early leaf-on (May to June), Mid leaf-on (July to August) and Late leaf-on (September to October) variability in P_r; the pattern is shown qualitatively in Figure 10. Dormant (November to February) and pre-budburst (March to April) P_r are also shown as these influence the perched water table at the site and ground water reservoirs, both of which we know may be utilised by old growth oak (). The wettest and driest years and leaf-on seasons in respect of the tree hydraulic year are also marked. During the growing season P_r averages 499 mm (Table 6) with the preceding dormant season typically providing about 50% of the precipitation in the plant hydraulic year. Year 2 of the study (2017–2018) was the driest hydraulic year overall despite a very wet pre-budburst and both Year 0 (2015–2016) and Year 5 (2020–2021) were the wettest. Year 0 also had very wet early leaf-on season. The three leaf-on periods (defined in Table 1) provide maximum canopy interception. For the treatment season, monthly throughfall (P_f, mm), i.e. average precipitation received at soil level, and monthly interception (P_i, mm), are shown in Fig. 11, across the five treatment years by year. By comparing reference precipitation April–October with the treatment season throughfall (P_{fs}, %) results, monthly and treatment season total interception percentage (P_{is}, %) can also be deduced. Treatment season throughfall averages 59% per month. Annual throughfall averages 64% across the five years presented.

Throughfall percentages are of course influenced by changes to canopy cover, for example due to defoliation by herbivory, which were recorded in May 2018 & 2019, but the evidence from Fig. 11 is not conclusive. Another driver of high throughfall is heavy rain, for example in July and October 2019 and June and August 2020. To fully assess these factors LAI data is required which was not available for all years of this study. In this study we have visualised correlations in environmental influences (Fig.S8) and compared monthly precipitation to all-tree *TWU* (Fig. S9) but not completed any full analyses through modelling.

FACE Treatment season label		Reference Precipitation P_r (mm)						
Year		2016	2017	2018	2019	2020	2021	Mean
Annual (Jan-Dec)		871.3	713.2	625.9	758.9	741.3	780.7	748.6
Tree hydraulic year		2015-6	2016-7	2017-8	2018-9	2019-20	2020-21	
Annual (Nov-Oct) % anomaly to mean 2015-2021		913.5 22.3	720.9 -3.5	649.2 -13.1	718.2 -3.9	721.4 -3.4	759.3 1.6	747.1 0.0
November – Feb	Dormant	296.6	273.4	225.7	151.9	244.3	296.3	248.0
March – April	Pre-budburst	153.6	68.3	178.2	74.4	34.2	35.7	90.7
May – June	Early leaf-on	202.3	106.2	61.5	160.3	123.0	134.0	131.2
July – August	Mid leaf-on	153.9	157.4	64.5	130.8	198.4	116.5	136.9
September – October	Late leaf-on	107.1	115.6	119.4	200.8	121.6	176.8	140.2
March – Oct	Growing	616.9	447.4	423.5	566.4	477.1	463.0	499.1

Table : Precipitation totals and percentage deviations from mean across the seasons and years of interest. 2016 (2015/2016) included as a pre-treatment year. Calendar years are shown in rows 1-2; hydraulic year is used in the remainder of the table. Underline is maximum and underline is minimum of the years.

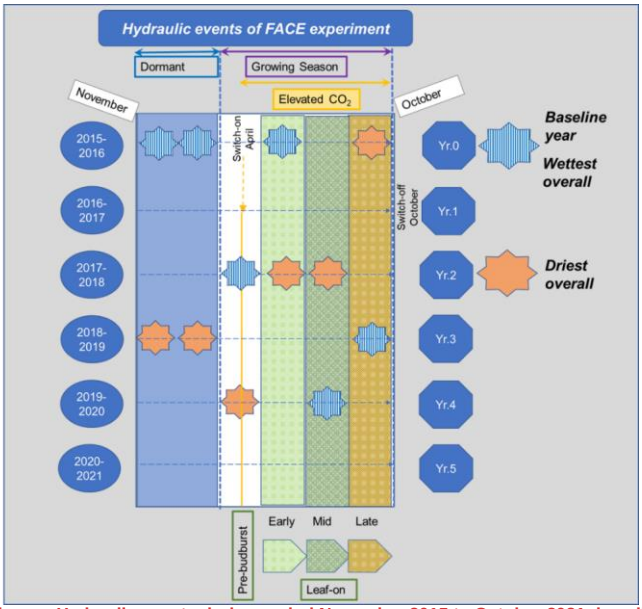

610 **Figure : Hydraulic events during period November 2015 to October 2021, baseline Year 0 and Years 1 to 5 of the FACE experiment. Year 2 (2017–2018) was the driest hydraulic year overall and year 4 (2019–2020) was the wettest including a very wet mid leaf-on season.**

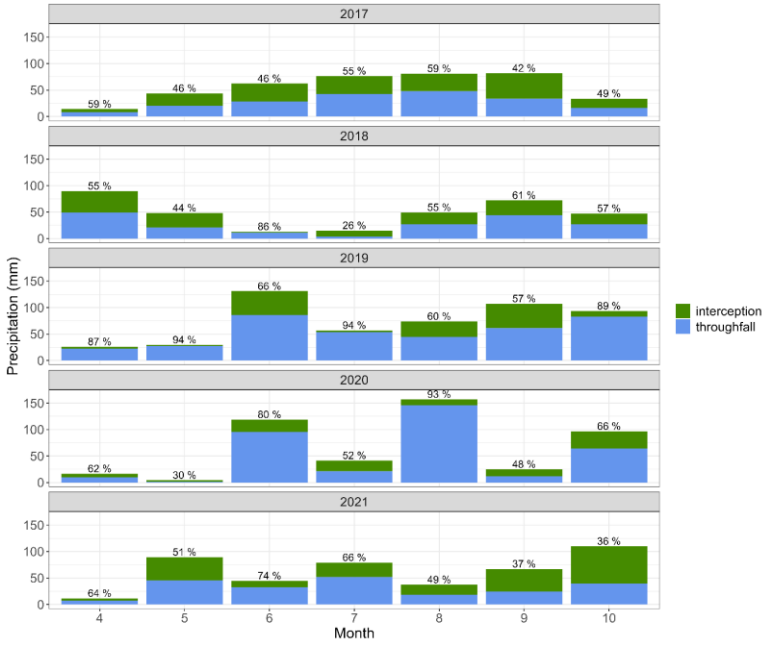

Figure : Local monthly precipitation, shown as stacked throughfall (P_f mm) and interception (P_i mm), at BIFoR FACE for treatment seasons 2017 to 2021. Percentage throughfall is indicated above each combined bar.

3.5.2 Shallow soil moisture response to treatment season precipitation

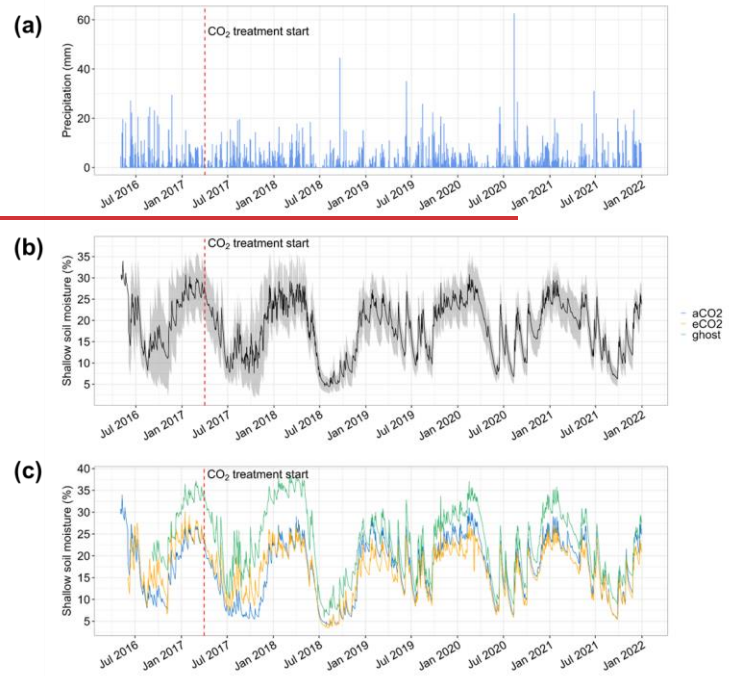

Figure : Years 2016–2021 (a) daily precipitation (b) daily shallow soil moisture + sd averaged across all treatment arrays (c) daily mean shallow soil moisture by treatment. Extended from MacKenzie et al., 2021.

Throughfall during the treatment season (Fig. 11) directly affects Volumetric Water Content (VWC) and may therefore influence *TWU* from budburst to senescence. The extent of shallow (0 to 20cm depth) soil moisture depletion during drought and its effects on water usage by BIFoR FACE control (*aCO₂* and *Ghost*) oaks has been reported by Rabbai et al. (2023). Shallow soil moisture availability decreases progressively across the leaf-on season even in wet summers (and Fig. 12). During herbivore attack especially in 2018 and 2019 () a smaller canopy interception (and smaller leaf area) can be assumed to affect leaf-on total water usage interactively.

Comparing Figs. 8 and 12, the opposite seasonalities of *TWU* and VWC are evident with autumn–winter dormant season providing VWC recharge. Tree water usage drives the leaf-on seasonal reduction in VWC, although the leaf season VWC cycle is strongly modulated by precipitation (e.g., Fig.12, summer 2020). On shorter, sub-seasonal and daily timescales, the relationship between *TWU* and VWC is not expected to be simple. We defer a full account of sub-seasonal *TWU* v. VWC relations to future work, but note here in passing that, for example during the most pronounced continuous dry period of the observation period (June to July 2018, Fig. 12), there appears to be no inter-year difference in median *Ghost* tree diurnal sap flux (Fig. 5(a)), 95%ile sap flux (Fig. S5), or median *TWU* ((Fig. S6) in all *Ghost* trees.

~~3.6~~3.5 Discussion of tree water usage in the FACE experiment.

~~We have found a linear relationship between *TWU* and R_b for the summer (mid leaf-on) months, with only slightly differing slopes for the two infrastructure treatments as discussed in section 3.2 above. This finding has enabled normalisation of the water usage by tree size, so that the resulting TWU_n is suitable for hypothesis testing.~~

~~These~~Normalised water usage (section 3.2 above), TWU_n, is suitable for testing treatment hypotheses. The water usage results extend those from previous eCO_2 studies of oak (e.g., Leuzinger and Körner, 2007) by being over of a longer duration of treatment (numbers of years and numbers of treatment days per year) and a greater size range and sample of trees.

~~3.6.1~~3.5.1 TWU_n differences under eCO_2

Table 4 reports reductions in mean eCO_2 TWU_n compared to aCO_2 TWU_n. Across whole growing seasons, the average percentage reduction in 2019 and 2021 is 16.5% (overall average 12% if the marginally significant reduction in 2020 is included). The largest TWU_n season-average reduction in Table 4 is 19% but we observe substantial interannual variability~~.~~ most probably related to differing precipitation and light level amounts. These tests confirm our hypothesis 1 over whole seasons, whilst July-only results are less conclusive.

We are not aware of other whole-growing-season oak results with which to compare these TWU_n results. Each treatment TWU_n is a proxy for stand transpiration so we next compare our FACE results to eCO_2 : control transpiration ratios from previous FACE experiments of oak and other deciduous species .

Short duration mid-summer FACE results have been reported for mature temperate broadleaves. Leuzinger and Körner (2007) were unable to statistically test species specific differences in transpiration for adult *Q. petraea* (Matt.) Liebl. under eCO_2 in their web-FACE experiment but found a 14% reduction overall when results for *Q. petraea* were pooled with those of *Carpinus betulus* L., and *Fagus sylvatica* L. in summers 2004 and 2005. Their Web-FACE operated under a similar CO_2 elevation (ambient is not reported) to that used at BIFoR FACE. Our July-only TWU_n results (reductions in every year but only significantly so for the 26% reduction in 2019) for *Q. robur* differ from their results for *Q. petraea* but strengthen their overall conclusions regarding adult deciduous broadleaves, and regarding the large interannual variability they also observe.

Both seasonal and summer results at ORNL are reported by Warren et al. (2011a) for 11,16 and 20-year-old *Liquidambar styraciflua* L. in years 1999, 2004 and 2008 and in early 2007 season by Warren et al. (2011b). Again similar FACE CO_2 elevation was used as at BIFoR FACE. ORNL ambient CO_2 levels were 380–400 μmol mol^{-1} giving a ca. 40% elevation compared to our current ca. 35%. Warren et al. (2011a, their Table III) report 10–16% seasonal reductions in stand transpiration under eCO_2 which increased with year of treatment. This may reflect a differing species response to eCO_2. For summer only, a 7–16% reduction was reported, whilst Warren et al. (2011b, their Fig. 1) report ca. 28% reductions in the (non-drought) first half of a single growing season at the same ORNL site. This again reflects large interannual summer response variability.

The reductions in TWU_n in our study are consistent with other treatment effects seen at BIFoR FACE: diurnal results for photosynthetic enhancement (23 ± 4% higher for eCO_2, Gardner et al., 2022); and fine root production (45% higher for eCO_2 in the first two years (Ziegler et al., 2023) although not specifically targeted at the focal TWU_n trees and covering whole year rather than season only). Synthesis of these treatment effects into quantitative budgets for water and carbon is outside the scope of the present work.

~~3.6.2~~3.5.2 FACE infrastructure effect on TWU_n.

The effect of FACE infrastructure on tree water usage has not to our knowledge been previously reported. TWU_n was lower for the *Ghost* trees compared to infrastructure control aCO_2 trees across the three treatment years analysed, 2019–2021. In 2019, 2020 and 2021 seasons, we found a consistently significant 37% to 20% increase in mean aCO_2 TWU_n compared with *Ghost* TWU_n (Fig. 9, Table 5). Similar consistently significant results hold for July-only TWU_n results 2019–2021. These tests confirm our hypothesis 2.

The results of this study indicate the importance of infrastructure controls in forest FACE experiments. The greater aCO_2 TWU_n may be due to one or more of several factors: effects of FACE infrastructure gas injection on air mixing and turbulence and hence changes in microclimate; differences in ground cover; or array-specific differences in soil moisture, slope, soil respiration, or species of sub-dominant trees present. ~~The higher TWU_n and lower soil moisture levels in both types of infrastructure arrays in comparison with no-infrastructure arrays are consistent (Fig. 12(c)).~~Further work is needed to fully explore the soil moisture results.

Since the treatment effect for eCO_2 is of opposite sign to that for infrastructure, (i.e. we see a reduction in eCO_2 TWU_n compared with aCO_2 TWU_n, but an increase in aCO_2 TWU_n compared with *Ghost* TWU_n) the infrastructure treatment effect cannot cause a pseudo-eCO_2 effect in the statistics, but it does reduce our certainty about the absolute magnitude of the eCO_2 effect.

~~3.7~~3.6 Capabilities, limitations and usability of sap flux data from HPC probesets

Although this experiment had relatively small sample size (total 18 trees, six per treatment), it was nevertheless a substantive experiment consisting of 12,259 days of individual tree data (770,667 diurnal sap flux measurements) in a unique experimental setting, making this dataset of high value for modellers of dynamic vegetation, water, and climate. We have defined a parameter TWU_n to enable consistent water usage comparisons between individual trees and hence treatments diurnally across both summer months and whole seasons. We consider that this method of processing HPC sap flux results, along with the extensive and continuous dataset for all no-infrastructure *Ghost* control trees over more than four years, gives us high confidence in this normalised data.

We can clearly demonstrate that use of four thermocouple positions across the sapwood for each of our HPC probesets has enabled us to capture successfully the position and size of point sap flux density (derived from sap velocity) and that this has given us a more reliable basis to explore the effects of tree size on both whole-probeset sap flux and *TWU*. With respect to sap flux, single probesets are unlikely to provide representative results of *TWU* due to asymmetry in sapwood radial width around the circumference of the tree. The effects of time-out value in the HPC measurement system have been discussed (Appendix B) and recommendations are made to ensure any repeat experiments using this technique consider truncation effects for diurnal sap flux. Here the diurnal truncated distributions have been accumulated to *TWU* and analysed using one-way ANOVA which gave sufficient confidence to enable testing of the two hypotheses.

4 Conclusions

Water usage was calculated from stem sap flux for 18 oaks in an old growth even-aged plantation during five years of eCO_2. The oaks were distributed across the three treatment conditions eCO_2, aCO_2 and *Ghost*. Diurnal (i.e. daylight) responses accumulated over days, months, and growing seasons (April–October inclusive) were the focus. Within a given year, median, mean and extreme (95%ile) diurnal sap flux increased in the spring from first leaf to achieve peak daily values in summer months (July, August)). We accumulated sap flux daily to derive water usage information for each tree, averaging results from two probesets per tree to eliminate orientation imbalances.

Differences in tree water usage varied according to tree size. Tree characteristics, R_b and A_c, were measured and correlated linearly with mean diurnal water usage, ***TWU***, for July confirming a recent study (Schoppach et al., 2021). The linear relationship between A_c and ***TWU*** is less certain than that between R_b and ***TWU*** but can be used to convert tree-based transpiration to a stand scale (Granier et al., 2000; Poyatos et al., 2016) for comparison with dynamic vegetation and climate models.

Normalisation of *TWU* by R_b, to give TWU_n, enabled comparison of data combined from multiple trees across the treatments. A growing-season reduction in TWU_n under eCO_2 was detected; the signal was less clear for July-only data. There was considerable interannual variability in the treatment effect for growing-season and July-only averages, likely related to environmental drivers but which remains to be diagnosed or modelled fully. Sub-seasonal and shorter timescale variability also remains to be explored more fully.

Growing-season and July-only increases in TWU_n under aCO_2 compared to non-infrastructure controls (*Ghost* trees) were detected consistently in all years, showing either that the presence of infrastructure affects water usage, or the *Ghost* positions are not comparable to those of the infrastructure arrays due to array-specific differences in soil moisture, slope, soil respiration or sub-dominant tree species presence.

Whilst the experiment produced reliable data across the five years, outlier incidence appears to be increasing, and re-installation of probesets is recommended. To detect cavitation and embolism in situ, as a possible cause of outlier data, separate (e.g. acoustic) monitoring would be required. Whilst much further work remains, this first set of tree water usage results strongly supports the conclusion that old growth oak forests conserve water under eCO_2 at the whole-plant level.

5 Appendix A: Additional tables

Symbol	Description	Units used in this publication (* not SI)
A_c	Canopy area (i.e. the area of ground covered by a plant canopy)	m^2
A_{sw}	Cross-sectional sapwood area *	cm^2
A_z	Annular ring cross-sectional area at thermocouple z	cm^2
F_L	volume fraction of water element of xylem woody matrix	unitless
F_M	volume fraction of wood element of xylem woody matrix	unitless
Gs	canopy stomatal conductance	mm s-1
H	heartwood radius	m
J	Sap flux density	$m\ s^{-1}$
J_z	Point sap flux density across xylem sapwood area at measurement point. Unit derivation: m^3 (water) m^{-2}(xylem sapwood area) s^{-1}	$m\ s^{-1}$
P	Precipitation	mm
P_r	Local precipitation (outside forest).	Mm
P_{fs}	Throughfall estimate within treatment season April–Oct	%
P_{is}	Interception estimate within treatment season April–Oct	%
Q_p	Probeset volumetric sap flux (across sapwood)	litres s^{-1}
Q_T	Whole tree sap flux density	litres s^{-1}
R	cambium radius	m
R_b	Bark radius	mm
r_z	radius of measurement point within sap transducer (z =1 to 4).	M
T_a	Temperature	^{o}C
TG	Total solar radiation	Watt m^{-2}
TWU	Tree diurnal (dawn to dusk) water usage per day	litres d^{-1}
TWU	Monthly mean *TWU*	litres d^{-1} $month^{-1}$
TWU_n	Tree diurnal (dawn to dusk) water usage per day normalised by bark radius at the point of probeset insertion, R_b (mm).	litres d^{-1} mm^{-1}
TWU_n	Monthly mean TWU_n	litres d^{-1} mm^{-1} $month^{-1}$
t_z	Time to heat balance point for one thermocouple pair position (z =1 to 4) in the xylem sap Compensated Heat Pulse (CMP) probeset data	seconds
V_s	Raw heat velocity (uncompensated)	$m\ s^{-1}$
V_c	Wound compensated heat velocity	$m\ s^{-1}$
X_d	Vertical distance between heater probe and upper (downstream) sap sensor probe	mm
X_u	Vertical distance between heater probe and upper (downstream) sap sensor probe	mm
Statistical term abbreviations SE – standard error, adjusted R^2 – adjusted coefficient of determination, t – student's t-test statistic, df – degrees of freedom, p – significance.		

Table A1: Table of parameter symbols and statistical abbreviations.

Stage	Parameter	Relationship equation	References
Stage 1	t_z **Time to heat balance point**	At each position z = 1 to 4	Tranzflo Manual
Stage 2	V_s **Raw heat velocity (uncompensated)**	At each position z = 1 to 4 $$Vs = \left\{\frac{(Xd+Xu)}{2tz}\right\} \quad (A1)$$ For long probes X_d = 20, X_u = 5 in mm V_s = 12.5 / t_z	Swanson, 1962 Tranzflo Manual
Stage 3	V_c **Wound compensated heat velocity**	At each position z = 1 to 4 $$Vc = a + bV + cV^2 + dV^3 \quad (A2)$$ Where V is V_s in m s^{-1}. Empirical parameters *a, b, c and d* are chosen for probe diameter 2 mm.	Green and Clothier, 1988
Stage 4	J_z **Probeset (4 point) Sap flux density for each radius transducer position**	$$J_z = \{(0.505\ F_M + F_L)V_{c,z}\}; z = 1{:}4 \quad (A3)$$ Where J_z **is the sap flux density** at each position z = 1 to 4 Defining conversion factor c1 as $$c1 = (0.505\ F_M + F_L) \quad (A4)$$ gives $$J = c1\ V_{c,z} \quad (A5)$$	Edwards and Warwick, 1984; Marshall, 1958
Stage 5	Q_p **Probeset Volumetric Sap flux across sapwood**	**For each probeset** $$Q_P = \sum_{z=1}^{z=4} A_z J_z;\ \text{p=E (east) or W(west)} \quad (A6)$$ Area-weighted sum of sap flux density, where associated sapwood areas, A_z *for z = 1 to 4* for long probes, is calculated from *R*, r_z, r_{z+1},… r_{z+3} (radii) and *H*.	Hatton et al., 1990; Tranzflo Manual
Stage 6	Q_T **Whole tree Sap flux**	**For each probeset at each sample time:** ***(Qp1+ Qp2)/2 simplified model*** $$Q_T = \frac{(Q_E + Q_W)}{2} \quad (A7)$$ Where E and W indicate east -facing and west-facing probes.	
Stage 7	***TWU*** **Tree diurnal water usage**	$$TWU = N\sum_{i=idawn}^{i=idusk} Q_{Ti} \quad (A8)$$ Where *i* is the 30-minute sample time of Q_{Ti}, N is conversion factor from per second (***Q_T)*** to per diurnal day dawn to dusk	

Table A2: Calculations stages 1 to 7 showing flow of data processing to obtain *TWU* from time to heat balance t_z from all differential HPC probeset thermocouple radial positions.

735

6 Appendix B: Limitations of the time-out characteristic and outliers

There are known limitations in the ability of the HPC system to measure low and reverse sap velocities (Forster, 2017) and to some extent high sap velocities (Burgess et al., 2001). With respect to our set up, we optimised the high end of this limitation by choosing suggested sensor spacings recommended by a manufacturer, Tranzflo, with extensive experience in a wide range of deciduous trees. The limitations of the time-out characteristic and the effect this places on HPC data are recorded in several references (e.g. see Tranzflo: Measurements of Sap Flow by the Heat-Pulse Method. An Instruction Manual for the HPV system, 2016). The limitations impact on our choice of data processing (e.g. diurnal versus diel) and feed through into the statistics we report. These limitations also introduce a truncation effect at lower heat velocities so that the distribution of the resulting raw and processed data is not symmetrical. We had limited options to extend the time-out period due to the multiple types of data needing to be captured by our single logger/ multiplexer arrangement in each array.

To normalise the data, given the above time-out effect, we select only those daylight periods where we can be confident that all four thermocouples are measuring and where they exhibit a shaped maximum point sap flux density value. We also focus on accumulation and percentile ranges rather than point time results. It is possible to use fewer positions for our calculations if, for example, one probeset position is giving a constant truncated value. These instances would need individual verification.

There were limited options to extend the time-out period for the combination of Tranzflo probeset system and Campbell Scientific logger/ multiplexer used in this project. Based on our experience, extending the time-out beyond double (i.e. beyond 660 second = 11 minutes) would be impractical for the current set-up. Extension beyond, say, 7 minutes (420 seconds) would likely require a decrease to the sampling frequency to 1 s (currently set to 0.5 s) to ensure sufficient memory is available during the differential calculation period. This decrease in sampling frequency is an inevitable compromise between capturing low heat velocities and offering sufficient data discrimination to capture variation in heat velocity towards the maxima of the daily cycle.

7 Appendix C: Details of xylem sap flow measurements and calculations

In each research array a datalogger and multiplexer (CR1000+AM25T, Campbell Scientific, Logan, Utah, USA) was used for year-round 24-hour capture of raw data from sap flux HPC probesets manufactured by Tranzflo (New Zealand), soil and throughfall measurement devices.

The logger was programmed for data capture using CRBasicEditor under LoggerNet (versions to 4.6.2), also by Campbell Scientific, Logan, Utah, USA. We tested our prototype installation set-up in mid-summer 2017 to determine if we could capture the expected range of heat velocities and applied similar capture programs to all array loggers.

Each target oak tree had two probesets, East- and West-facing, using long (7 cm four-sensor) probes. Each probeset was inserted at a stem height between 1.1 and 1.3 m and contained a central heat pulse probe and two measurement probes (each containing four thermocouples for long probes respectively) upstream and downstream of the heater (Fig. 2). Transducers were positioned radially in the stem (to suit the ring-porous characteristics and bark thickness of old growth *Q.robur*). Each probeset was protected from natural heating by reflective insulation covers during the treatment season.

During monitoring, a heater pulse of duration 1.5–2.5 secs was applied half-hourly through a heater box (one per tree) to the heater probes. The pulse duration was dependant on the number of heaters pulsed simultaneously. A 2 second pulse was standard for the two oak per array (four long probeset) configuration. Each thermocouple pair in the upstream and downstream positions took up to 330sec (5.5 minutes) to reach a differential heat balance

point and this time determined the minimum detectable heat velocity, for a time just within this timeout period. The thermocouple datalogger sampling rate of 0.5 secs determined the maximum detectable speed (minimum time-to-balance), which, given normal interference levels, was adequate for deriving maximum heat velocity. 16 differential thermocouple configurations were sampled per array in one 6 minute timeslot every 30 minutes, giving time-to-balance t_z data in seconds.

Data collection problems, due to logger earthing and sap probe misconnections at manufacture, caused data loss early in the project. Contact with sapwood was maintained for all oak trees from installation to March 2021, when two out of the 36 probesets failed.

7.1 Raw file processing

Logger data from the nine C1000 FACE research loggers were collated by array and transducer type (i.e. 7 cm probeset datasets for oaks only) using 'R', then combined into year files for further data processing.

7.2 Xylem sap flux calculations.

Following quality checks, each stage of calculation to produce wound-corrected sap velocity and sap flux density at each transducer position (four per probeset) was performed in stages (see Table A2). Table A2 lists the methodology and equations along with associated literature sources for each stage.

At stage 3 (Table A2), the Green and Clothier (1988) polynomial factors were used for wound compensation. For stage 4, the conversion factor c1 was derived by measurement of wet and dry woodcores and microcores (Eq.(A4) and Eq.(A5)) to calculate xylem sap velocity from heat velocity in oakwood ~~(Edwards and Warwick, 1984;). Measurement of wet and dry woodcores and microcores previously described provided data for derivation~~.

Short incremental wood cores (circa 10 cm long, 4 mm diameter) were taken from two old growth oaks outside of the experimental arrays. Microcores were also taken near all 36 target oak probeset installation positions. These cores were used to determine wood hydraulic properties (Edwards and Warwick, 1984; Marshall, 1958) for sap velocity and flux calculations (see stage 4, Table A2 and definitions Table A1). In summer 2021 woodcores taken from some of the target oaks were further analysed to check the conversion (xylem woody matrix) factors from heat velocity to sap velocity and to verify the active xylem radial width. The visibly active xylem (sapwood) is typically between seven and 50 mm when viewed in wet cores. The uncertainty in heartwood boundary H (m), as described in Appendix B, could be resolved in future similar studies by taking short cores prior to installing instrumentation.

7.2.1 Heat pulse to xylem sap flux calculations.

Figure C1 shows example positional (i.e. thermocouple-specific), point sap flux density data from four probesets in two trees ~~Figure C1 illustrates~~ illustrating positioning of peak sap flux through the sapwood ~~in two trees~~. Figure C1(a) pools results from both trees. Data from the thermocouple radial position giving the highest diurnal values (one thermocouple position for each probeset) are selected from the four-position data and shown across a 24-hour period (Fig. C1(a)). The diurnal maxima from the larger Tree 1 are larger than those for the smaller Tree 2. Figure C1(b) pools probeset results from the larger tree, E-facing (top) and W-facing (bottom). Note the increase in sap flux density towards the centre of the sapwood, decreasing again towards the heartwood (Fig. C1(b)).

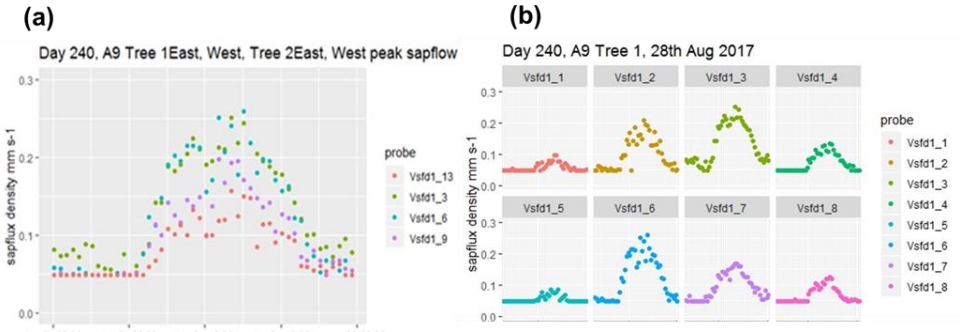

Figure C1: a) Example Stage 4 output showing peak point sap flux density in two trees for one sunny day in August 2017. Tree 1 (vsfd1_3 and vsfd1_6) bark radius is larger than Tree 2 (vsfd1_9 and vsfd_13). b) Example Stage 4 output showing changes to point sap flux density across the active xylem for E facing (top) and W facing (bottom) probesets of one tree (Tree 1) on the same day in August 2017. The lefthand probe position is nearest to the bark and the righthand probeset position is nearest to the heartwood. Note the peak value occurs at different sensor positions for the two probesets.

The nocturnal/ pre-dawn response for the smaller tree in 1(a) (vsfd1_9 and vsfd_13)) and the less vigorous thermocouple positions in the larger tree in Figure C1(b) (vsfd1_1, vsfd_4, vsfd1_5 and vsfd_8) have their minima determined by the previously mentioned time-out limit (i.e. t_z of 330 secs). These minima do not affect the processing of diurnal values but influence nocturnal value accuracy of the lowest point sap flux density (see Appendix B). The radial pattern of sap flux density increases in amplitude to a peak position within the probeset measurement zone and then decreases again towards the heartwood boundary as depth from the cambium increases (Fig. C1(a) and (b)), a characteristic of these ring porous oak species. The radial amplitude patterns vary across seasons.

7.3 Converting point xylem sap flux data to whole tree water usage.

An adapted simple integration method (Hatton et al. 1990), based on a weighted average approach was used where the point sap flux density is weighted by the areas of the annular rings associated with each r_z. Fig. C1. Hatton et al. (1990) consider their method, in comparison with alternatives (e.g. fitting a least-squares polynomial), a simpler and more accurate approach for estimation of the volume flux.

Using cambium radius (*R*) data, estimated heartwood radius (*H)* (0.05 m smaller than the inner sensor radial position), along with transducer radius positions (r_z), point sap flux density from the four measurements points is converted to volumetric (half tree) total sap flux for each probeset (Fig. 3) by using the integration of the point sap fluxes over the active sapwood conducting area (Stage 5, Appendix Table A2 and Appendix C).

8 Code availability

R code for sap flux and *TWU* data analysis and logger CSBasic programs, can be requested from the correspondence author (ARM) or the first author (SEQ). R code for the precipitation and soil moisture data is available at https://github.com/giuliocurioni/Sue_paper1/invitations.

9 Data availability

All data used to carry out this study are available upon request via the correspondence author (RMK); this includes both logged data and physical tree measurements/ ecological information for example. Sap flux data are available at UBIRA eData repository doi. https://doi.org/10.25500/edata.bham.00000972

Phenocam data available https://phenocam.nau.edu/webcam/roi/millhaft/DB_1000/

10 Supplement link: the link to the supplement will be included by Copernicus, if applicable.

11 Author contribution:

SEQ designed and carried out the sap flow investigation and prepared the manuscript as part of the FACE programme designed by ARM. SEQ installed sap instrumentation, programmed the data loggers, curated, visualised and analysed the sap data, manually collected, visualised and analysed woodcores and physical tree data. NH reviewed the logger software, provided initial raw data visualisation, designed and reported on all array CO_2 monitoring and installed/ managed the FACE data network and local server. GC and NH curated the raw FACE engineering data. GC curated and visualised the reference and on-site weather data, as well as all core soil data, supported by the FACE team. ARM and SK supervised the project. All co-authors discussed the results and contributed to the finalised manuscript.

Conceptualization SEQ, RMK, BIFoR FACE team ,
Data curation SEQ, GC, NH
Formal analysis SEQ
Investigation, Methodology, Project administration SEQ
Resources RMK, BIFOR team
Software SEQ , NH
Supervision RMK, SK
Visualization SEQ, GC, NH
Writing original draft preparation SEQ. Review & editing primarily SEQ supported by RMK, SK, GC

12 Competing interests:

"The authors declare that they have no conflict of interest."

13 Special issue statement: the statement on a corresponding special issue will be included by Copernicus, if applicable.

14 Acknowledgements

All authors acknowledge support from the Birmingham Institute of Forest Research. BIFoR FACE facility is a research infrastructure project supported by the JABBS Foundation and the University of Birmingham. ARM gratefully acknowledges support from NERC (grant nos. NE/S015833/1 and NE/S002189/1). SEQ acknowledges BIFoR FACE Operations team's contribution to logger and instrumentation implementation, data visualisation and data curation. Laboratories and workshops were provided at BIFoR FACE. Special thanks to Neil Loader (University of Swansea) for supporting Trephor microcorer usage, for wood core analysis and dendrochronological dating of trees. Thanks go to Ian Phillips for advice on statistical analysis. Acknowledgement to Woodland Trust and the Centre for Ecology and Hydrology for enabling use of site phenology data collected 2016-2022 for submission to Nature's Calendar by SEQ as a citizen scientist. Shawbury historical precipitation data provided by the National Meteorological Library and Archive – Met Office, UK.

15 References

Aranda, I., Forner, A., Cuesta, B., and Valladares, F.: Species-specific water use by forest tree species: From the tree to the stand, Agric. Water Manag., 114, 67–77, https://doi.org/10.1016/J.AGWAT.2012.06.024, 2012.

Asgharinia, S., Leberecht, M., Belelli Marchesini, L., Friess, N., Gianelle, D., Nauss, T., Opgenoorth, L., Yates, J., and Valentini, R.: Towards Continuous Stem Water Content and Sap Flux Density Monitoring: IoT-Based Solution for Detecting Changes in Stem Water Dynamics, https://doi.org/10.3390/f13071040, 2022.

Aszalós, R., Horváth, F., Mázsa, K., Ódor, P., Lengyel, A., Kovács, G., and Bölöni, J.: First signs of old-growth structure and composition of an oak forest after four decades of abandonment, Biologia (Bratisl)., 72, 1264–1274, https://doi.org/10.1515/biolog-2017-0139, 2017.

Baldocchi, D., Falge, E., Gu, L., Olson, R., Hollinger, D., Running, S., Anthoni, P., Bernhofer, C., Davis, K., Evans, R., Fuentes, J., Goldstein, A., Katul, G., Law, B., Lee, X., Malhi, Y., Meyers, T., Munger, J., Oechel, W., and Richardson, F.: FLUXNET: A New Tool to Study the Temporal and Spatial Variability of Ecosystem–Scale Carbon Dioxide, Water Vapor, and Energy Flux Densities, ©2001 Am. Meteorol. Soc., 82, https://doi.org/10.1175/1520-0477(2001)082<2415:FANTTS>2.3.CO;2, 2001.

Baldocchi, D. D., Black, T. A., Curtis, P. S., Falge, E., Fuentes, J. D., Granier, A., Gu, L., Knohl, A., Pilegaard, K., Schmid, H. P., Valentini, R., Wilson, K., Wofsy, S., Xu, L., and Yamamoto, S.: Predicting the onset of net carbon uptake by deciduous forests with soil temperature and climate data: A synthesis of FLUXNET data, Int. J. Biometeorol., https://doi.org/10.1007/s00484-005-0256-4, 2005.

Bradwell, J.: Norbury Park An Estate Tackling Climate Change., Second edi., Norbury Park, Staffordshire, UK, 2022.

Brodribb, T. J., Skelton, R. P., McAdam, S. A. M., Bienaimé, D., Lucani, C. J., and Marmottant, P.: Visual quantification of embolism reveals leaf vulnerability to hydraulic failure, New Phytol., 209, 1403–1409, https://doi.org/10.1111/nph.13846, 2016.

Burgess, S. S. O., Adams, M. A., Turner, N. C., Beverly, C. R., Ong, C. K., Khan, A. A. H., and Bleby, T. M.: An improved heat pulse method to measure low and reverse rates of sap flow in woody plants†, Tree Physiol., 21, 589–598, 2001.

Bütikofer, L., Anderson, K., Bebber, D. P., Bennie, J. J., Early, R. I., and Maclean, I. M. D.: The problem of scale in predicting biological responses to climate, Glob. Chang. Biol., n/a, https://doi.org/10.1111/gcb.15358, 2020.

Catoni, R., Gratani, L., Sartori, F., Varone, L., and Granata, M. U.: Carbon gain optimization in five broadleaf deciduous trees in response to light variation within the crown: Correlations among morphological, anatomical and physiological leaf traits, Acta Bot. Croat., 74, 71–94, https://doi.org/10.1515/botcro-2015-0010, 2015.

Catovsky, S., Holbrook, N. M., and Bazzaz, F. A.: Coupling whole-tree transpiration and canopy photosynthesis in coniferous and broad-leaved tree species, Can. J. For. Res., 32, 295–309, 2002.

Čermak, J., KUČERA, J., and ŠTĚPÁNKOVÁ, M.: Water consumption of full-grown oak (Quereus robur L.) in a floodplain forest after the cessation of flooding, https://doi.org/10.1016/b978-0-444-98756-3.50034-4, 1991.

Chave, J.: The problem of pattern and scale in ecology: what have we learned in 20 years?, Ecol. Lett., 16, 4–16, https://doi.org/10.1111/ele.12048, 2013.

Choat, B., Brodribb, T. J., Brodersen, C. R., Duursma, R. A., López, R., and Medlyn, B. E.: Triggers of tree mortality under drought, Nature, 558, 531–539, https://doi.org/10.1038/s41586-018-0240-x, 2018.

David, T. S., Pinto, C. A., Nadezhdina, N., Kurz-Besson, C., Henriques, M. O., Quilhó, T., Cermak, J., Chaves, M. M., Pereira, J. S., and David, J. S.: Root functioning, tree water use and hydraulic redistribution in Quercus suber trees: A modeling approach based on root sap flow, For. Ecol. Manage., 307, 136–146, https://doi.org/10.1016/j.foreco.2013.07.012, 2013.

Dietrich, L., Zweifel, R., and Kahmen, A.: Daily stem diameter variations can predict the canopy water status of mature temperate trees, Tree Physiol., https://doi.org/10.1093/treephys/tpy023, 2018.

Donohue, R. J., Roderick, M. L., McVicar, T. R., and Yang, Y.: A simple hypothesis of how leaf and canopy-level transpiration and assimilation respond to elevated CO 2 reveals distinct response patterns between disturbed and undisturbed vegetation, J. Geophys. Res. Biogeosciences, https://doi.org/10.1002/2016JG003505, 2017.

Dragoni, D., Caylor, K. K., and Schmid, H. P.: Decoupling structural and environmental determinants of sap velocity: Part II. Observational application, Agric. For. Meteorol., 149, 570–581, https://doi.org/10.1016/j.agrformet.2008.10.010, 2009.

Drake, J. E., Macdonald, C. A., Tjoelker, M. G., Crous, K. Y., Gimeno, T. E., Singh, B. K., Reich, P. B., Anderson, I. C., and Ellsworth, D. S.: Short-term carbon cycling responses of a mature eucalypt woodland to gradual stepwise enrichment of atmospheric CO2 concentration, Glob. Chang. Biol., 22, 380–390, https://doi.org/10.1111/gcb.13109, 2016.

Edwards, W. R. N. and Warwick, N. W. M.: Transpiration from a kiwifruit vine as estimated by the heat pulse technique and the penman-monteith equation, New Zeal. J. Agric. Res., https://doi.org/10.1080/00288233.1984.10418016, 1984.

Ellsworth, D. S.: CO2 enrichment in a maturing pine forest: are CO2 exchange and water status in the canopy affected?, Plant. Cell Environ., 22, 461–472, https://doi.org/10.1046/j.1365-3040.1999.00433.x, 1999.

Fan, Y., Miguez-Macho, G., Jobbágy, E. G., Jackson, R. B., and Otero-Casal, C.: Hydrologic regulation of plant rooting depth, Proc. Natl. Acad. Sci. U. S. A., 114, 10572–10577, https://doi.org/10.1073/pnas.1712381114, 2017.

Flo, V., Martínez-Vilalta, J., Mencuccini, M., Granda, V., Anderegg, W. R. L., and Poyatos, R.: Climate and functional traits jointly mediate tree water-use strategies, New Phytol., 231, 617–630, https://doi.org/10.1111/nph.17404, 2021.

Fontes, C. G. and Cavender-Bares, J.: Toward an integrated view of the 'elephant': unlocking the mysteries of water transport and xylem vulnerability in oaks, Tree Physiol., 40, 1–4, https://doi.org/10.1093/treephys/tpz116, 2019.

Forster, M.: How Reliable Are Heat Pulse Velocity Methods for Estimating Tree Transpiration?, 8, 350, https://doi.org/10.3390/f8090350, 2017.

Gao, J. and Tian, K.: Stem and leaf traits as co-determinants of canopy water flux., Plant Divers., 41(4):, 258-265., 2019.

Gardner, A., Ellsworth, D. S., Crous, K. Y., Pritchard, J., and MacKenzie, A. R.: Is photosynthetic enhancement sustained through three years of elevated CO2 exposure in 175-year-old Quercus robur?, Tree Physiol., 42, 130–144, https://doi.org/10.1093/treephys/tpab090, 2022.

Granier, A., Biron, P., BRÉDA, N., PONTAILLER, J.-Y., and SAUGIER, B.: Transpiration of trees and forest stands: short and long-term monitoring using sapflow methods, Glob. Chang. Biol., 2, 265–274, https://doi.org/10.1111/j.1365-2486.1996.tb00078.x, 1996.

Granier, A., Loustau, D., and Bréda, N.: A generic model of forest canopy conductance dependent on climate, soil water availability and leaf area index, Ann. For. Sci., 57, 755–765, https://doi.org/10.1051/forest:2000158, 2000.

Green, S. R. and Clothier, B. E.: Water use of kiwifruit vines and apple trees by the heat-pulse technique, J. Exp. Bot., 39, 115–123, https://doi.org/10.1093/jxb/39.1.115, 1988.

Grossiord, C., Buckley, T. N., Cernusak, L. A., Novick, K. A., Poulter, B., Siegwolf, R. T. W., Sperry, J. S., and McDowell, N. G.: Plant responses to rising vapor pressure deficit, https://doi.org/10.1111/nph.16485, 2020.

Guerrieri, R., Lepine, L., Asbjornsen, H., Xiao, J., and Ollinger, S. V.: Evapotranspiration and water use efficiency in relation to climate and canopy nitrogen in U.S. forests, J. Geophys. Res. Biogeosciences, https://doi.org/10.1002/2016JG003415, 2016.

Hart, K. M., Curioni, G., Blaen, P., Harper, N. J., Miles, P., Lewin, K. F., Nagy, J., Bannister, E. J., Cai, X. M., Thomas, R. M., Krause, S., Tausz, M., and MacKenzie, A. R.: Characteristics of free air carbon dioxide enrichment of a northern temperate mature forest, Glob. Chang. Biol., 26, 1023–1037, https://doi.org/10.1111/gcb.14786, 2020.

Hassler, S. K., Weiler, M., and Blume, T.: Tree-, stand- and site-specific controls on landscape-scale patterns of transpiration, Hydrol. Earth Syst. Sci., 22, 13–30, https://doi.org/10.5194/hess-22-13-2018, 2018.

Hatton, T. J., Catchpole, E. A., and Vertessy, R. A.: Integration of sapflow velocity to estimate plant water use, Tree Physiol., 6, 201–209, https://doi.org/10.1093/treephys/6.2.201, 1990.

Herbst, M., Roberts, J. M., Rosier, P. T. W., Taylor, M. E., and Gowing, D. J.: Edge effects and forest water use: A field study in a mixed deciduous woodland, For. Ecol. Manage., 250, 176–186, https://doi.org/10.1016/j.foreco.2007.05.013, 2007.

Huete, A., Justice, C., and Liu, H.: Development of vegetation and soil indices for MODIS-EOS, Remote Sens. Environ., 49, 224–234, https://doi.org/10.1016/0034-4257(94)90018-3, 1994.

IPCC: Summary for Policymakers. In: Climate Change 2021: The Physical Science Basis. Contribution of Working Group I to the Sixth Assessment Report of the Intergovernmental Panel on Climate Change [Masson-Delmotte, V., P. Zhai, A. Pirani, S.L. Connors, C. Péan, 2021.

Iqbal, S., Zha, T., Jia, X., Hayat, M., Qian, D., Bourque, C. P.-A., Tian, Y., Bai, Y., Liu, P., Yang, R., and Khan, A.: Interannual variation in sap flow response in three xeric shrub species to periodic drought, Agric. For. Meteorol., 297, 108276, https://doi.org/10.1016/j.agrformet.2020.108276, 2021.

De Kauwe, M. G., Medlyn, B. E., Zaehle, S., Walker, A. P., Dietze, M. C., Hickler, T., Jain, A. K., Luo, Y., Parton, W. J., Prentice, I. C., Smith, B., Thornton, P. E., Wang, S., Wang, Y.-P., Wårlind, D., Weng, E., Crous, K. Y., Ellsworth, D. S., Hanson, P. J., Seok Kim, H.-, Warren, J. M., Oren, R., and Norby, R. J.: Forest water use and water use efficiency at elevated CO2: a model-data intercomparison at two contrasting temperate forest FACE sites, Glob. Chang. Biol., 19, 1759–1779, https://doi.org/10.1111/gcb.12164, 2013.

Keenan, T. F., Hollinger, D. Y., Bohrer, G., Dragoni, D., Munger, J. W., Schmid, H. P., and Richardson, A. D.: Increase in forest water-use efficiency as atmospheric carbon dioxide concentrations rise, Nature, 499, 324–327, https://doi.org/10.1038/nature12291, 2013.

Landsberg, J., Waring, R., and Ryan, M.: Water relations in tree physiology: where to from here?, Tree Physiol., 37, 18–32, https://doi.org/10.1093/treephys/tpw102, 2017.

Lavergne, A., Sandoval, D., Hare, V. J., Graven, H., and Prentice, I. C.: Impacts of soil water stress on the acclimated stomatal limitation of photosynthesis: Insights from stable carbon isotope data, Glob. Chang. Biol., n/a, https://doi.org/10.1111/gcb.15364, 2020.

LeCain, D., Smith, D., Morgan, J., Kimball, B. A., Pendall, E., Miglietta, F.: Microclimatic Performance of a Free-Air Warming and CO2 Enrichment Experiment in Windy Wyoming, USA., 10:, https://doi.org/10.1371/journal.pone.0116834, 2015.

Lemeur, R., Fernández, J. E. and Steppe, K. .: Symbols, SI units and physical quantities within the scope of sap flow studies, Acta Hortic., (846), 21–32, n.d.

Leuzinger, S. and Körner, C.: Water savings in mature deciduous forest trees under elevated CO2, Glob. Chang. Biol., 13, 2498–2508, https://doi.org/10.1111/j.1365-2486.2007.01467.x, 2007.

Leuzinger, S., Zotz, G., Asshoff, R., and Körner, C.: Responses of deciduous forest trees to severe drought in Central Europe, Tree Physiol., 25, 641–650, https://doi.org/10.1093/treephys/25.6.641, 2005.

Levene, H.: No Title, in: Contributions to Probability and Statistics: Essays in Honor of Harold Hotelling, edited by: Olkin, I. et al., Stanford University Press, 278–292, 1960.

Li, J. ‐ H., Dugas, W. A., Hymus, G. J., Johnson, D. P., Hinkle, C. R., Drake, B. G., and Hungate, B. A.: Direct and indirect effects of elevated CO2 on transpiration from Quercus myrtifolia in a scrub ‐ oak ecosystem, Glob. Chang. Biol., 9, 96 ‐ 105, https://doi.org/10.1046/j.1365-2486.2003.00557.x, 2003.

MacKenzie, A. R., Krause, S., Hart, K. M., Thomas, R. M., Blaen, P. J., Hamilton, R. L., Curioni, G., Quick, S. E., Kourmouli, A., Hannah, D. M., Comer-Warner, S. A., Brekenfeld, N., Ullah, S., and Press, M. C.: BIFoR FACE: Water–soil–vegetation–atmosphere data from a temperate deciduous forest catchment, including under elevated CO2, Hydrol. Process., 35, e14096, https://doi.org/10.1002/hyp.14096, 2021.

Marshall, D. C.: Measurement of Sap Flow in Conifers by Heat Transport., Plant Physiol., 33, 385 LP – 396, https://doi.org/10.1104/pp.33.6.385, 1958.

Martínez-Sancho, E., Treydte, K., Lehmann, M. M., Rigling, A., and Fonti, P.: Drought impacts on tree carbon sequestration and water use – evidence from intra-annual tree-ring characteristics, New Phytol., n/a, https://doi.org/10.1111/nph.18224, 2022.

McGill, R., Tukey, J. W., and Larsen, W. A.: Variations of Box Plots, Am. Stat., 32, 12–16, https://doi.org/10.2307/2683468, 1978.

Medlyn, B. E., Zaehle, S., De Kauwe, M. G., Walker, A. P., Dietze, M. C., Hanson, P. J., Hickler, T., Jain, A. K., Luo, Y., Parton, W., Prentice, I. C., Thornton, P. E., Wang, S., Wang, Y.-P., Weng, E., Iversen, C. M., McCarthy, H. R., Warren, J. M., Oren, R., and Norby, R. J.: Using ecosystem experiments to improve vegetation models, Nat. Clim. Chang., 5, 528–534, 2015.

Miglietta, F., Peressotti, A., Vaccari, F. P., Zaldei, A., DeAngelis, P., and Scarascia-Mugnozza, G.: Free-air CO2 enrichment (FACE) of a poplar plantation: the POPFACE fumigation system, New Phytol., 150, 465–476, https://doi.org/10.1046/j.1469-8137.2001.00115.x, 2001.

Moene, A. F.: Vegetation: Transport Processes Inside and Outside of Plants, in: Transport in the Atmosphere-Vegetation-Soil Continuum, edited by: Moene, A. F. and Dam, J. C. van, Cambridge University Press, Cambridge, 200–251, https://doi.org/DOI: 10.1017/CBO9781139043137.007, 2014.

Montagnoli, A.: Adaptation of the Root System to the Environment, https://doi.org/10.3390/f13040595, 2022.

Nehemy, M. F., Benettin, P., Asadollahi, M., Pratt, D., Rinaldo, A., and McDonnell, J. J.: Tree water deficit and dynamic source water partitioning, Hydrol. Process., 35, e14004, https://doi.org/10.1002/hyp.14004, 2021.

Niinemets, Ü. and Valladares, F.: TOLERANCE TO SHADE, DROUGHT, AND WATERLOGGING OF TEMPERATE NORTHERN HEMISPHERE TREES AND SHRUBS, Ecol. Monogr., 76, 521–547, https://doi.org/10.1890/0012-9615(2006)076[0521:TTSDAW]2.0.CO;2, 2006.

Norby, R. J., De Kauwe, M. G., Domingues, T. F., Duursma, R. A., Ellsworth, D. S., Goll, D. S., Lapola, D. M., Luus, K. A., Mackenzie, A. R., Medlyn, B. E., Pavlick, R., Rammig, A., Smith, B., Thomas, R., Thonicke, K., Walker, A. P., Yang, X., and Zaehle, S.: Model-data synthesis for the next generation of forest free-air CO2 enrichment (FACE) experiments, New Phytol., https://doi.org/10.1111/nph.13593, 2016.

Perkins, D., Uhl, E., Biber, P., Du Toit, B., Carraro, V., Rötzer, T., and Pretzsch, H.: Impact of Climate Trends and Drought Events on the Growth of Oaks (Quercus robur L. and Quercus petraea (Matt.) Liebl.) within and beyond Their Natural Range, https://doi.org/10.3390/f9030108, 2018.

Philip, J. R.: Plant Water Relations: Some Physical Aspects, Annu. Rev. Plant Physiol., 17, 245–268, https://doi.org/10.1146/annurev.pp.17.060166.001333, 1966.

Pinter, P. J., Kimball, B. A., Wall, G. W., LaMorte, R. L., Hunsaker, D. J., Adamsen, F. J., Frumau, K. F. A., Vugts, H. F., Hendrey, G. R., Lewin, K. F., Nagy, J., Johnson, H. B., Wechsung, F., Leavitt, S. W., Thompson, T. L., Matthias, A. D., and Brooks, T. J.: Free-air CO2 enrichment (FACE): blower effects on wheat canopy microclimate

and plant development, Agric. For. Meteorol., 103, 319–333, https://doi.org/10.1016/S0168-1923(00)00150-7, 2000.

Poyatos, R., Granda, V., Flo, V., Adams, M., Adorján, B., Aguadé, D., P.M, A., Allen, S., Alvarado-Barrientos, M., Anderson-Teixeira, K., Luiza, M., Aparecido, L. M., Arain, M., Aranda, I., Asbjornsen, H., Baxter, R., Beamesderfer, E., Berry, Z., Berveiller, D., and Oliveira, R.: Global transpiration data from sap flow measurements: the SAPFLUXNET database, Earth Syst. Sci. Data, essd-2020-, https://doi.org/10.5194/essd-2020-227, 2020.

Quick, S : Research data supporting the publication 'Water usage of old growth oak at elevated CO_2 in the FACE of climate change', University of Birmingham UBIRA [dataset], https://doi.org/10.25500/edata.bham.00000972, 2023.

Rabbai, A., Wendt, D. E., Curioni, G., Quick, S. E., MacKenzie, A. R., Hannah, D. M., Kettridge, N., Ullah, S., Hart, K. M., and Krause, S.: Soil moisture and temperature dynamics in juvenile and mature forest as a result of tree growth, hydrometeorological forcings, and drought, Hydrol. Process., 37, e14919, https://doi.org/10.1002/hyp.14919, 2023.

Renner, M., Hassler, S. K., Blume, T., Weiler, M., Hildebrandt, A., Guderle, M., Schymanski, S. J., and Kleidon, A.: Dominant controls of transpiration along a hillslope transect inferred from ecohydrological measurements and thermodynamic limits, Hydrol. Earth Syst. Sci., 20, 2063–2083, https://doi.org/10.5194/hess-20-2063-2016, 2016.

Robert, E., Mencuccini, M., and Martinez Vilalta, J.: The Anatomy and Functioning of the Xylem in Oaks, 261–302, https://doi.org/10.1007/978-3-319-69099-5_8, 2017.

Roberts, A. J., Crowley, L. M., Sadler, J. P., Nguyen, T. T. T., Gardner, A. M., Hayward, S. A. L., and Metcalfe, D. B.: Effects of Elevated Atmospheric CO2 Concentration on Insect Herbivory and Nutrient Fluxes in a Mature Temperate Forest, 13, https://doi.org/10.3390/f13070998, 2022.

RStudio Team: RStudio: Integrated Development Environment for R., http://www.rstudio.com/., 2022.

Salomón, R. L., Peters, R. L., Zweifel, R., Sass-Klaassen, U. G. W., Stegehuis, A. I., Smiljanic, M., Poyatos, R., Babst, F., Cienciala, E., Fonti, P., Lerink, B. J. W., Lindner, M., Martinez-Vilalta, J., Mencuccini, M., Nabuurs, G.-J., van der Maaten, E., von Arx, G., Bär, A., Akhmetzyanov, L., Balanzategui, D., Bellan, M., Bendix, J., Berveiller, D., Blaženec, M., Čada, V., Carraro, V., Cecchini, S., Chan, T., Conedera, M., Delpierre, N., Delzon, S., Ditmarová, Ľ., Dolezal, J., Dufrêne, E., Edvardsson, J., Ehekircher, S., Forner, A., Frouz, J., Ganthaler, A., Gryc, V., Güney, A., Heinrich, I., Hentschel, R., Janda, P., Ježík, M., Kahle, H.-P., Knüsel, S., Krejza, J., Kuberski, Ł., Kučera, J., Lebourgeois, F., Mikoláš, M., Matula, R., Mayr, S., Oberhuber, W., Obojes, N., Osborne, B., Paljakka, T., Plichta, R., Rabbel, I., Rathgeber, C. B. K., Salmon, Y., Saunders, M., Scharnweber, T., Sitková, Z., Stangler, D. F., Stereńczak, K., Stojanović, M., Střelcová, K., Světlík, J., Svoboda, M., Tobin, B., Trotsiuk, V., Urban, J., Valladares, F., Vavrčík, H., Vejpustková, M., Walthert, L., Wilmking, M., Zin, E., Zou, J., and Steppe, K.: The 2018 European heatwave led to stem dehydration but not to consistent growth reductions in forests, Nat. Commun., 13, 28, https://doi.org/10.1038/s41467-021-27579-9, 2022.

Sánchez-Costa, E., Poyatos, R., and Sabaté, S.: Contrasting growth and water use strategies in four co-occurring Mediterranean tree species revealed by concurrent measurements of sap flow and stem diameter variations, Agric. For. Meteorol., 207, 24–37, https://doi.org/10.1016/j.agrformet.2015.03.012, 2015.

Sánchez-Pérez, J. M., Lucot, E., Bariac, T., and Trémolières, M.: Water uptake by trees in a riparian hardwood forest (Rhine floodplain, France), Hydrol. Process., https://doi.org/10.1002/hyp.6604, 2008.

Sass-Klaassen, U., Sabajo, C. R., and den Ouden, J.: Vessel formation in relation to leaf phenology in pedunculate oak and European ash, 29, 171–175, https://doi.org/10.1016/j.dendro.2011.01.002, 2011.

Schäfer, K. V. R.: Canopy Stomatal Conductance Following Drought, Disturbance, and Death in an Upland Oak/Pine Forest of the New Jersey Pine Barrens, USA , https://www.frontiersin.org/articles/10.3389/fpls.2011.00015, 2011.

Schäfer, K. V. R., Oren, R., Lai, C.-T. C.-T., Katul, G. G., Schäfer, K. V. R., Oren, R., Lai, C.-T. C.-T., and Katul, G. G.: Hydrologic balance in an intact temperate forest ecosystem under ambient and elevated atmospheric CO 2 concentration, Glob. Chang. Biol., 8, 895–911, 2002.

Schoppach, R., Chun, K. P., He, Q., Fabiani, G., and Klaus, J.: Species-specific control of DBH and landscape characteristics on tree-to-tree variability of sap velocity, Agric. For. Meteorol., 307, 108533, https://doi.org/10.1016/j.agrformet.2021.108533, 2021.

Schreel, J. D. M., von der Crone, J. S., Kangur, O., and Steppe, K.: Influence of Drought on Foliar Water Uptake Capacity of Temperate Tree Species, 10, 562, https://doi.org/10.3390/f10070562, 2019.

Sperry, J. S.: Evolution of Water Transport and Xylem Structure, Int. J. Plant Sci., 164, S115–S127, https://doi.org/10.1086/368398, 2003.

Stagge, J. H., Kingston, D. G., Tallaksen, L. M., and Hannah, D. M.: Observed drought indices show increasing divergence across Europe, Sci. Rep., 7, 14045, https://doi.org/10.1038/s41598-017-14283-2, 2017.

Steppe, K. and Lemeur, R.: Effects of ring-porous and diffuse-porous stem wood anatomy on the hydraulic parameters used in a water flow and storage model, Tree Physiol., https://doi.org/10.1093/treephys/27.1.43, 2007.

Steppe, K., von der Crone, J. S., and De Pauw, D. J. W.: TreeWatch.net: A Water and Carbon Monitoring and Modeling Network to Assess Instant Tree Hydraulics and Carbon Status , https://www.frontiersin.org/article/10.3389/fpls.2016.00993, 2016.

Sulman, B. N., Roman, D. T., Yi, K., Wang, L., Phillips, R. P., and Novick, K. A.: High atmospheric demand for water can limit forest carbon uptake and transpiration as severely as dry soil, Geophys. Res. Lett., https://doi.org/10.1002/2016GL069416, 2016.

Süßel, F. and Brüggemann, W.: Tree water relations of mature oaks in southwest Germany under extreme drought stress in summer 2018, Plant Stress, 1, 100010, https://doi.org/10.1016/j.stress.2021.100010, 2021.

Swanson, R. H.: An instrument for detecting sap movement in woody plants /, An Instrum. Detect. sap Mov. woody plants /, https://doi.org/10.5962/bhl.title.80872, 1962.

Tatarinov, F. a, Kučera, J., and Cienciala, E.: The analysis of physical background of tree sap flow measurement based on thermal methods, Meas. Sci. Technol., 16, 1157–1169, https://doi.org/10.1088/0957-0233/16/5/016, 2005.

Tor-ngern, P., Oren, R., Ward, E. J., Palmroth, S., McCarthy, H. R., and Domec, J.-C.: Increases in atmospheric CO2 have little influence on transpiration of a temperate forest canopy, New Phytol., 205, 518–525, https://doi.org/10.1111/nph.13148, 2015.

Tranzflo: Measurements of Sap Flow by the Heat-Pulse Method. An Instruction Manual for the HPV system: https://www.tranzflo.co.nz/index_files/HPVMANUAL.PDF, last access: 12 October 2016, 1998.Tricker, P. J., Pecchiari, M., Bunn, S. M., Vaccari, F. P., Peressotti, A., Miglietta, F., and Taylor, G.: Water use of a bioenergy plantation increases in a future high CO2 world, https://doi.org/10.1016/j.biombioe.2008.05.009, 2009.

Uddling, J., Teclaw, R. M., Kubiske, M. E., Pregitzer, K. S., and Ellsworth, D. S.: Sap flux in pure aspen and mixed aspen–birch forests exposed to elevated concentrations of carbon dioxide and ozone, Tree Physiol., 28, 1231–1243, https://doi.org/10.1093/treephys/28.8.1231, 2008.

Valentini, R.: EUROFLUX: An Integrated Network for Studying the Long-Term Responses of Biospheric Exchanges of Carbon, Water, and Energy of European Forests, 163, 1–8, https://doi.org/10.1007/978-3-662-05171-9_1, 2003.

Venturas, M. D., Sperry, J. S., and Hacke, U. G.: Plant xylem hydraulics: What we understand, current research, and future challenges, https://doi.org/10.1111/jipb.12534, 2017.

Verstraeten, W. W., Veroustraete, F., and Feyen, J.: Assessment of Evapotranspiration and Soil Moisture Content Across Different Scales of Observation, 8, 70–117, https://doi.org/10.3390/s8010070, 2008.

Vitasse, Y., Bottero, A., Cailleret, M., Bigler, C., Fonti, P., Gessler, A., Lévesque, M., Rohner, B., Weber, P., Rigling, A., and Wohlgemuth, T.: Contrasting resistance and resilience to extreme drought and late spring frost in five major European tree species, Glob. Chang. Biol., 25, 3781–3792, https://doi.org/10.1111/gcb.14803, 2019.

Volkmann, T. H. M., Kühnhammer, K., Herbstritt, B., Gessler, A., and Weiler, M.: A method for in situ monitoring of the isotope composition of tree xylem water using laser spectroscopy, Plant. Cell Environ., n/a-n/a, https://doi.org/10.1111/pce.12725, 2016.

Wang, H., Guan, H., and Simmons, C. T.: Modeling the environmental controls on tree water use at different temporal scales, Agric. For. Meteorol., 225, 24–35, https://doi.org/10.1016/j.agrformet.2016.04.016, 2016.

Warren, J. M., Pötzelsberger, E., Wullschleger, S. D., Thornton, P. E., Hasenauer, H., and Norby, R. J.: Ecohydrologic impact of reduced stomatal conductance in forests exposed to elevated CO2, 4, 196–210, https://doi.org/doi:10.1002/eco.173, 2011a.

Warren, J. M., Norby, R. J., and Wullschleger, S. D.: Elevated CO2 enhances leaf senescence during extreme drought in a temperate forest, Tree Physiol., 31, 117–130, https://doi.org/10.1093/treephys/tpr002, 2011b.

Wehr, R., Commane, R., Munger, J. W., McManus, J. B., Nelson, D. D., Zahniser, M. S., Saleska, S. R., and Wofsy, S. C.: Dynamics of canopy stomatal conductance, transpiration, and evaporation in a temperate deciduous forest, validated by carbonyl sulfide uptake, 14, 389–401, https://doi.org/10.5194/bg-14-389-2017, 2017.

Wickham, H.: ggplot2: Elegant Graphics for Data Analysis., 2016.

Wiedemann, A., Marañón-Jiménez, S., Rebmann, C., Herbst, M., and Cuntz, M.: An empirical study of the wound effect on sap flux density measured with thermal dissipation probes, Tree Physiol., 36, 1471–1484, 2016.

Wullschleger, S. D. and Norby, R. J.: Sap velocity and canopy transpiration in a sweetgum stand exposed to free-air CO2 enrichment (FACE), New Phytol., 150, 489–498, https://doi.org/10.1046/j.1469-8137.2001.00094.x, 2001.

Wullschleger, S. D., Gunderson, C. A., Hanson, P. J., Wilson, K. B., and Norby, R. J.: Sensitivity of stomatal and canopy conductance to elevated CO2 concentration – interacting variables and perspectives of scale, New Phytol., 153, 485–496, https://doi.org/10.1046/j.0028-646X.2001.00333.x, 2002.

Xu, X. and Trugman, A. T.: Trait-Based Modeling of Terrestrial Ecosystems: Advances and Challenges Under Global Change, Curr. Clim. Chang. Reports, 7, 1–13, https://doi.org/10.1007/s40641-020-00168-6, 2021.

Ziegler, C., Kulawska, A., Kourmouli, A., Hamilton, L., Shi, Z., MacKenzie, A. R., Dyson, R. J., and Johnston, I. G.: Quantification and uncertainty of root growth stimulation by elevated CO2 in a mature temperate deciduous forest, Sci. Total Environ., 854, 158661, https://doi.org/10.1016/j.scitotenv.2022.158661, 2023.